Available online at www.sciencedirect.com
SCIENCE DIRECT®
ELSEVIER
International Journal of Solids and Structures 43 (2006) 583–612
INTERNATIONAL JOURNAL OF SOLIDS and STRUCTURES
www.elsevier.com/locate/ijsolstr

An energy release rate-based plastic-damage model for concrete

Jian Ying Wu [a,1], Jie Li [b,*], Rui Faria [c]

[a] *Department of Civil Engineering, College of Architecture & Civil Engineering, South China University of Technology, Guangzhou 200092, China*
[b] *Department of Building Engineering, Tongji University, Shanghai 200092, China*
[c] *Faculdade de Engenharia da Universidade do Porto, Civil Engineering Department, Rua Dr. Roberto Frias s/n, 4200-465 Porto, Portugal*

Received 25 September 2004; received in revised form 17 May 2005
Available online 18 July 2005

Abstract

A new plastic-damage constitutive model for concrete is proposed in this paper. A tensile and a shear damage variable are adopted to describe the degradation of the macromechanical properties of concrete. Within the framework of continuum damage mechanics, the elastic Helmholtz free energy is defined to establish the plastic-damage constitutive relation with the internal variables. Regarding the specific format for the effective stress space plasticity, the evolution law for the plastic strains and the explicit expression for the elastoplastic Helmholtz free energy are determined and the damage energy release rates that are conjugated to the damage variables are derived. Thus, damage energy release rate-based damage criteria can be established in conformity to thermodynamical principles. In accordance with the normality rule, evolution laws for the damage variables are obtained to complete the proposed plastic-damage model. Some computational aspects concerning the numerical algorithm implementation are discussed as well. Several numerical simulations are presented at the end of the paper, whose results allow for validating the capability of the proposed model for reproducing the typical nonlinear performances of concrete structures under different monotonic and cyclic load conditions.

Keywords: Continuum damage mechanics; Damage criteria; Plastic deformations; Concrete; Thermodynamics

* Corresponding author. Tel.: +86 2165979519; fax: +86 2165986345.
E-mail addresses: jywu@scut.edu.cn (J.Y. Wu), lijie@mail.tongji.edu.cn (J. Li).
[1] Fax: +86 20 87114632.

0020-7683/$ - see front matter © 2005 Elsevier Ltd. All rights reserved.
doi:10.1016/j.ijsolstr.2005.05.038

1. Introduction

Despite the noteworthy recent research efforts and contributions, the task of nonlinear finite element analysis (NFEA) of concrete structures is still quite challenging. The accurate modeling of concrete performances, the key issue to NFEA, remains a somewhat controversial matter.

The most commonly used theories for the modeling of concrete are plasticity, fracture-based approaches and continuum damage mechanics (CDM). Plasticity, which has been successfully applied to metals, is nowadays theoretically consolidated and world-widely recognized as computationally efficient. Examples of its application to concrete can be found in Ohtani and Chen (1988), Etse and Willam (1994) and Feenstra and de Borst (1996), as well as in Chen (1994) reviews and references therein. Though the plasticity models are far superior to elastic approaches in representing hardening and softening characteristics, they fail to address the process of damage due to microcracks growth, such as the stiffness degradation, the unilateral effect, etc.

Intermingled with classical continuum mechanics in uncoupled manner, fracture mechanics suggests an approach to describe localized damage as to be represented by the ideal or regular discrete cracks with definite geometries and locations, and it has been extensively used in engineering practice (Krajcinovic, 1985). However, the associated questions whether the J integrals and stress intensity factors are material parameters or not are far from being settled (Yazdani and Schreyer, 1990). Besides, before the appearance of macrocracks in concrete there exist a lot of smeared microcracks whose geometries and locations could not be determined precisely, so it appears difficult to apply fracture mechanics for modeling concrete.

Based on the thermodynamics of irreversible processes, the internal state variable theory and relevant physical considerations (Ju, 1989), CDM provides a powerful and general framework for the derivation of consistent constitutive models suitable for many engineering materials, including concrete. In the earlier literature (Mazars, 1984, 1985; Mazars and Pijaudier-Cabot, 1989), CDM was restricted to linear "elastic-damage" mechanics for brittle materials, i.e., linear elastic solids with distributed microcracks, affording different ways for handling observed phenomena like the stiffness degradation, the tensile softening and the unilateral effect due to the development of microcracks and microvoids. More examples of elastic CDM models for concrete can be found in Lubarda et al. (1994), Cervera et al. (1995), Halm and Dragon (1996), Comi and Perego (2001), etc.

Coupled with plasticity or by means of empirical definitions, the irreversible strains due to plastic flow can also be accounted for in elastoplastic damage theories, such as those proposed by Ortiz (1985), Lemaitre (1985), Dragon (1985), Resende (1987), Simo and Ju (1987), Yazdani and Schreyer (1990), Carol et al. (1994), di Prisco and Mazars (1996), Lee and Fenves (1998), Faria et al. (1998), Hatzigeorgioiu et al. (2001), Hansen et al. (2001) among others.

One of the critical issues associated with damage model of concrete is selection of damage criteria. Several different criteria, such as the equivalent strain-based (Mazars, 1984), and the stress-based approaches (Ortiz, 1985; Chow and Wang, 1987) as well as the damage energy release rate-based (DERR-based) proposals (Mazars, 1985; Simo and Ju, 1987; Ju, 1989), are generally adopted in the current practice. Among them, it has been pointed out that (Ju, 1989) the equivalent strain-based damage criteria are only appropriate for the elastic state, and the stress-based damage criteria are inherently inadequate for predicting perfect plastic damage growth. As is well known, in classical plasticity the stress tensor is thermodynamically conjugated to the plastic strain tensor, so the yield criteria are defined as functions of the stress tensor invariants. Analogously thermodynamically consistent damage criteria might be based on DERRs that are the conjugated forces to the damage variables.

However, most of the above referred damage models, except in Ju (1989), are based on the Helmholtz free energy (HFE) and the DERR proposed by Lemaitre (1985), where contribution of the plastic strains to the microcrack growth process is not considered, and the driving force of damage growth is the elastic DERR alone, which might not be physically appropriate. Therefore, if the damage criteria are based on the elastic DERRs, the strength enhancement observed in the compression–compression domain (Kupfer

et al., 1969) cannot be predicted [see the unilateral damage model of Mazars (1985)]. To deal with above problem, Ju (1989) suggested an elastoplastic one-scalar damage model in which both the plastic strains and the plastic HFE were defined based on the effective stress space plasticity to cope with the coupled effects between the damage evolutions and the plastic flow. However, only under very simple situations such as Von Mises plasticity with linear isotropic hardening, the plastic HFE was provided explicitly in the model, and for other plasticity models more appropriate for concrete, it could only be computed incrementally with numerical integration, which might be time-consuming and unsteady. Moreover, though the model is thermodynamically more reasonable, but only under uniaxial compression its predicted results might agree with experimental observations; and no examples for concrete under more complex stress states, e.g., biaxial compression, were provided yet.

To improve the fitting of the model predictions to the concrete experimental data, other researchers (Faria et al., 1998; Comi and Perego, 2001) abandoned the DERR-based damage criteria, and turned to the empirically defined ones. In spite of the satisfactory results obtained under pure tension and pure compression stress states, in the tension–compression domain the model of Faria et al. (1998) neglects the influence on the compressive strength in one direction due to the tensile stress or strain acting perpendicularly and vice versa, which is obviously conflicting with the experimentally observed strength decays (Kupfer et al., 1969; Vecchio and Collins, 1986). In Comi and Perego (2001) a pure elastic-damage model is proposed, where the damage criteria were described by a hyperbola for the tensile stress domains and an ellipse for the pure compressive stress quadrants. Many parameters with not very clear physical meaning are required to be determined in this model, and only under monotonic loadings the numerical results fit the experimental test data adequately.

With inspiration from all the previous works and understandings mentioned above, this paper aims to present a novel rate-independent plastic-damage model for concrete that should be consistent with thermodynamics and fit well with the concrete experimental observations, including the stiffness degradation, the enhancement of strength and ductility under compressive confinement, the strength decay induced by orthogonal tensile cracking and the unilateral effect under cyclic loading. The paper is organized as follows.

In Section 2 the peculiarities of the experimentally observed behaviour of concrete are reviewed. A tensile damage variable and a shear damage variable leading to a fourth-order damage tensor, are chosen to describe the degradation of the macromechanical properties of concrete. A decomposition of the effective stress tensor is presented thereafter to define an elastic HFE, after which the plastic-damage constitutive relation with internal variables is derived. Section 3 is devoted to the evolution laws for the internal variables. The evolution law for plastic strains is obtained and then the plastic HFE of concrete is determined. The elastic and plastic components of HFE are added up to the total elastoplastic one, from which the elastoplastic DERRs conjugated to the damage variables are derived to establish the damage criteria. Subsequently, in accordance with the normality rule, the evolution laws for the damage variables are obtained. Pertinent computational aspects concerning the numerical implementation and the algorithmic consistent tangent modulus for the constitutive model are presented in Section 4. In Section 5 some numerical applications of the model to experimental tests of concrete specimens and structures under different loadings are provided to validate and demonstrate the capability of the proposed model. Section 6 closes this paper with the most relevant conclusions.

2. Elastic-damage model

2.1. Damage mechanisms

To identify the basic mechanisms that lead to concrete damage growth, some primary features of concrete behaviour experimentally observed in tests are presented first.

When loaded in compression concrete experiences progressive loss of stiffness in the deviatoric space along with observed volumetric changes when approaching collapse putting into evidence strong dilatancy. The available experimental results in tension indicate a deviatoric behaviour similar to that observed in compression, but the volumetric performance, unlike in compression, is of a softening nature. Finally, under hydrostatic compression concrete exhibits somewhat softening behaviour at low stress levels, but as stress increases a predominantly stiffening behaviour is observed; upon unloading, concrete behaves almost elastically at first, losing stiffness progressively afterwards (Resende, 1987).

Consequently, three damage mechanisms can be consensually identified from the experimental observations, which are: (i) a tensile one, which represents the separation of material particles leading to cracks developed predominantly in fracture mode I; (ii) a shear one, inherent to mode II, associated to the breaking of internal bonds during the loading of concrete in shear; and finally (iii) a compressive consolidation one, due to collapse of the microporous structure of cement matrix under triaxial compression.

From these damage mechanisms it is possible to conclude that:

- Loaded in tension concrete damage is activated as the result of both the tensile and shear mechanisms in the deviatoric space. In general the former one develops much quicker than the latter one (Resende, 1987), and thus the shear damage mechanism can be ignored for convenience. In the volumetric space the damage of concrete is activated by the tensile damage mechanism.
- Loaded in compression concrete damage is activated by the shear damage mechanism. The compressive consolidation mechanism of concrete in the volumetric space will be partially taken into consideration via minor modification of the shear damage criteria, as it will be further discussed in Section 3 of the paper.

Thus, two basic but distinct mechanisms, namely the tensile and shear damage ones, respectively, are consistently referred to in the derivation of the constitutive model to be presented herein.

2.2. Types of damage models

The effectiveness and performance of a damage model depends heavily on its particular choice of a set of damage variables, which actually serves as a macroscopic approximation for describing the underlying micromechanical process of microcracking. In current literature, there are many ways to define appropriate damage variables which are phenomenologically defined or micromechanically derived. In this paper the attention is restricted to the phenomenological approach. According to the damage variables adopted, the CDM models can be classified essentially in two categories: (i) the scalar damage ones, where one or several scalars are adopted to characterize the isotropic damage processes (Mazars, 1984; Faria et al., 1998; Lee and Fenves, 1998; Hatzigeorgioiu et al., 2001); (ii) the tensor damage ones, where second-order, fourth-order or even eighth-order damage tensor are necessary to account for anisotropic damage effects (Ortiz, 1985; Dragon, 1985; Yazdani and Schreyer, 1990; Chaboche et al., 1995).

The one-scalar damage models (Mazars, 1984; Simo and Ju, 1987; Ju, 1989) are somewhat limited to describe the unilateral effect inherent to concrete behaviour. Moreover, Poisson's ratio is inferred to be a constant in this kind of damage model, which is inconsistent with the phenomena that Poisson's ratio decrease under tensile load and increase under compressive load due to microcracking. In fact, even for isotropic damage, not a one-scalar damage variable but at least a fourth-order damage tensor should be employed to characterize the state of damage in materials (Ju, 1990). However, the inherent complexities of numerical algorithms required by most of the anisotropic tensor damage models restrict their applicability to practical engineering.

Based on the considerations about the damage mechanisms discussed in Section 2.1, a tensile damage scalar d^+ and a shear damage scalar d^- will be adopted here to describe the degradation of the concrete macromechanical properties under tension and compression, respectively. As it will be shown, these two

damage scalars will lead to a fourth-order damage tensor, which agrees with the conclusion drawn in Ju (1990).

2.3. Decomposition of the effective stress tensor

In CDM the effective stress $\bar{\boldsymbol{\sigma}}$ in damaged material may be assumed to follow the classical elastoplastic behaviour (Ju, 1989; Faria et al., 1998), i.e.

$$\bar{\boldsymbol{\sigma}} = \mathbf{C}_0 : \boldsymbol{\varepsilon}^{\mathrm{e}} = \mathbf{C}_0 : (\boldsymbol{\varepsilon} - \boldsymbol{\varepsilon}^{\mathrm{p}}) \tag{1}$$

or equivalently

$$\boldsymbol{\varepsilon}^{\mathrm{e}} = \boldsymbol{\Lambda}_0 : \bar{\boldsymbol{\sigma}} \tag{2}$$

where $\mathbf{C}_0$ and $\boldsymbol{\Lambda}_0 = \mathbf{C}_0^{-1}$ denote the usual fourth-order isotropic linear-elastic stiffness and compliance tensors, respectively; $\boldsymbol{\varepsilon}$, $\boldsymbol{\varepsilon}^{\mathrm{e}}$ and $\boldsymbol{\varepsilon}^{\mathrm{p}}$ are rank-two tensors, denoting the strain tensor, its elastic and plastic tensor components.

To account for the different nonlinear performances of concrete under tension and compression, and to explicitly reproduce the dissimilar effects of the tensile and shear damage mechanisms, a decomposition of the effective stress tensor $\bar{\boldsymbol{\sigma}}$ into positive and negative components ($\bar{\boldsymbol{\sigma}}^+$, $\bar{\boldsymbol{\sigma}}^-$) is performed as (Ortiz, 1985; Ju, 1989; Faria et al., 1998)

$$\bar{\boldsymbol{\sigma}}^+ = \mathbf{P}^+ : \bar{\boldsymbol{\sigma}} \tag{3a}$$

$$\bar{\boldsymbol{\sigma}}^- = \bar{\boldsymbol{\sigma}} - \bar{\boldsymbol{\sigma}}^+ = \mathbf{P}^- : \bar{\boldsymbol{\sigma}} \tag{3b}$$

with the fourth-order projection tensors $\mathbf{P}^+$ and $\mathbf{P}^-$ expressed as (Faria et al., 2000)

$$\mathbf{P}^+ = \sum_i H(\bar{\sigma}_i)(\mathbf{p}_{ii} \otimes \mathbf{p}_{ii}) \tag{4a}$$

$$\mathbf{P}^- = \mathbf{I} - \mathbf{P}^+ \tag{4b}$$

where $\mathbf{I}$ is the fourth-order identity tensor; $H(\bar{\sigma}_i)$ denotes the Heaviside function computed for the ith eigenvalue $\bar{\sigma}_i$ of $\bar{\boldsymbol{\sigma}}$; and the second-order tensor $\mathbf{p}_{ii}$ will be defined in Eq. (7).

In order to express the rate format of the proposed model and to facilitate the derivation of the algorithmic consistent modulus, it is also necessary to split $\dot{\bar{\boldsymbol{\sigma}}}$ into its positive and negative components ($\dot{\bar{\boldsymbol{\sigma}}}^+$, $\dot{\bar{\boldsymbol{\sigma}}}^-$) as

$$\dot{\bar{\boldsymbol{\sigma}}}^+ = \frac{\mathrm{d}}{\mathrm{d}t}(\mathbf{P}^+ : \bar{\boldsymbol{\sigma}}) = \mathbf{Q}^+ : \dot{\bar{\boldsymbol{\sigma}}} \tag{5a}$$

$$\dot{\bar{\boldsymbol{\sigma}}}^- = \frac{\mathrm{d}}{\mathrm{d}t}(\mathbf{P}^- : \bar{\boldsymbol{\sigma}}) = \mathbf{Q}^- : \dot{\bar{\boldsymbol{\sigma}}} \tag{5b}$$

where the fourth-order tensors $\mathbf{Q}^+$ and $\mathbf{Q}^-$ are the corresponding projection tensors of $\dot{\bar{\boldsymbol{\sigma}}}$, and due to the nonlinear nature of $\mathbf{P}^+$ and $\mathbf{P}^-$, a somewhat more complicated procedure (refer to Faria et al., 2000 and see Appendix I for more discussions) is necessary to derive the expressions for them, leading to

$$\mathbf{Q}^+ = \mathbf{P}^+ + 2\sum_{i=1,j>i}^{3} \frac{\langle\bar{\sigma}_i\rangle - \langle\bar{\sigma}_j\rangle}{\bar{\sigma}_i - \bar{\sigma}_j}\mathbf{p}_{ij} \otimes \mathbf{p}_{ij} \tag{6a}$$

$$\mathbf{Q}^- = \mathbf{I} - \mathbf{Q}^+ \tag{6b}$$

To be used in Eqs. (4a) and (6), the second-order symmetric tensor $\mathbf{p}_{ij}$ should be defined as (see Faria et al., 2000 for details)

$$\mathbf{p}_{ij} = \mathbf{p}_{ji} = \tfrac{1}{2}(\mathbf{n}_i \otimes \mathbf{n}_j + \mathbf{n}_j \otimes \mathbf{n}_i) \tag{7}$$

where $\mathbf{n}_i$ is the ith normalized eigenvector corresponding to $\bar{\sigma}_i$; symbols $\langle\cdot\rangle$ are the McAuley brackets (ramp function) defined as

$$\langle x\rangle = (x + |x|)/2 \tag{8}$$

2.4. Elastic HFE potential

To establish the intended constitutive law, an elastic HFE potential should be introduced as function of the free and internal variables. The initial elastic HFE potential ψ_0^{e} is here defined as the elastic strain energy. It can be written as the addition of its positive and negative components ($\psi_0^{\mathrm{e}+}$, $\psi_0^{\mathrm{e}-}$) with the decomposition of the effective stress tensor given in Eqs. (3)

$$\psi_0^{\mathrm{e}}(\boldsymbol{\varepsilon}^{\mathrm{e}}) = \tfrac{1}{2}\bar{\boldsymbol{\sigma}} : \boldsymbol{\varepsilon}^{\mathrm{e}} = \tfrac{1}{2}\bar{\boldsymbol{\sigma}}^{+} : \boldsymbol{\varepsilon}^{\mathrm{e}} + \tfrac{1}{2}\bar{\boldsymbol{\sigma}}^{-} : \boldsymbol{\varepsilon}^{\mathrm{e}} = \psi_0^{\mathrm{e}+}(\boldsymbol{\varepsilon}^{\mathrm{e}}) + \psi_0^{\mathrm{e}-}(\boldsymbol{\varepsilon}^{\mathrm{e}}) \tag{9}$$

where superscript "e" refers to "elastic" and subscript "0" refers to "initial" states. $\psi_0^{\mathrm{e}+}$ and $\psi_0^{\mathrm{e}-}$ are further expressed as

$$\psi_0^{\mathrm{e}\pm}(\boldsymbol{\varepsilon}^{\mathrm{e}}) = \tfrac{1}{2}\bar{\boldsymbol{\sigma}}^{\pm} : \boldsymbol{\varepsilon}^{\mathrm{e}} = \tfrac{1}{2}\bar{\boldsymbol{\sigma}} : (\mathbf{P}^{\pm} : \boldsymbol{\Lambda}_0) : \ \bar{\boldsymbol{\sigma}} = \tfrac{1}{2}\boldsymbol{\varepsilon}^{\mathrm{e}} : (\mathbf{C}_0 : \mathbf{P}^{\pm}) : \ \boldsymbol{\varepsilon}^{\mathrm{e}} \tag{10}$$

with symbol "±" denoting "+" or "−", as appropriate.

Considering the tensile and shear damage mechanisms mentioned in Section 2.1, an elastic HFE potential with the form

$$\psi^{\mathrm{e}}(\boldsymbol{\varepsilon}^{\mathrm{e}}, d^+, d^-) = \psi^{\mathrm{e}+}(\boldsymbol{\varepsilon}^{\mathrm{e}}, d^+) + \psi^{\mathrm{e}-}(\boldsymbol{\varepsilon}^{\mathrm{e}}, d^-) \tag{11}$$

can be postulated, with $\psi^{\mathrm{e}+}$ and $\psi^{\mathrm{e}-}$ defined as

$$\psi^{\mathrm{e}\pm}(\boldsymbol{\varepsilon}^{\mathrm{e}}, d^{\pm}) = (1 - d^{\pm})\psi_0^{\mathrm{e}\pm}(\boldsymbol{\varepsilon}^{\mathrm{e}}) \tag{12}$$

2.5. Constitutive law and dissipation

In general, the total elastoplastic HFE potential can be defined as the sum of the elastic component ψ^{e} defined in Eqs. (10)–(12), and plastic component ψ^{p} to be defined in Section 3.2, assumed uncoupled in the following manner:

$$\psi(\boldsymbol{\varepsilon}^{\mathrm{e}}, \boldsymbol{\kappa}, d^+, d^-) = \psi^{\mathrm{e}}(\boldsymbol{\varepsilon}^{\mathrm{e}}, d^+, d^-) + \psi^{\mathrm{p}}(\boldsymbol{\kappa}, d^-) \tag{13}$$

where $\boldsymbol{\kappa}$ denotes a suitable set of plastic variables to be discussed in the next section.

On a purely isothermal mechanical process, the second principle of thermodynamics (Lubliner, 31972) states that any irreversible process should satisfy the Clausius–Duheim inequality, whose reduced form is

$$\dot{\gamma} = -\dot{\psi} + \boldsymbol{\sigma} : \ \dot{\boldsymbol{\varepsilon}} \geqslant 0 \tag{14}$$

By differentiating Eq. (13) with respect to time, one gets

$$\dot{\psi} = \frac{\partial \psi^{\mathrm{e}}}{\partial \boldsymbol{\varepsilon}^{\mathrm{e}}} : \dot{\boldsymbol{\varepsilon}}^{\mathrm{e}} + \frac{\partial \psi}{\partial d^+}\dot{d}^+ + \frac{\partial \psi}{\partial d^-}\dot{d}^- + \frac{\partial \psi^{\mathrm{p}}}{\partial \boldsymbol{\kappa}} \cdot \dot{\boldsymbol{\kappa}} \tag{15}$$

Referring to the standard thermodynamics arguments (Coleman and Gurtin, 1967), along with the assumption that damage and plastic unloading are elastic processes, for any admissible process the following conditions have to be fulfilled:

$$\boldsymbol{\sigma} = \frac{\psi^{\mathrm{e}}}{\partial \boldsymbol{\varepsilon}^{\mathrm{e}}} \tag{16}$$

$$\dot{\gamma}^{d} = -\left(\frac{\partial \psi}{\partial d^{+}}\dot{d}^{+} + \frac{\partial \psi}{\partial d^{-}}\dot{d}^{-}\right) \geqslant 0 \tag{17}$$

$$\dot{\gamma}^{\mathrm{p}} = \boldsymbol{\sigma} : \dot{\boldsymbol{\varepsilon}}^{\mathrm{p}} - \frac{\partial \psi^{\mathrm{p}}}{\partial \boldsymbol{\kappa}} \cdot \dot{\boldsymbol{\kappa}} \geqslant 0 \tag{18}$$

From Eq. (16) it can be clearly seen that the Cauchy stress tensor is only dependent on the elastic HFE potential, which is a variant to Faria et al. (1998) model where the total one are considered.

Considering the definition for the elastic HFE potential expressed in Eqs. (10)–(12), Eq. (16) leads to

$$\boldsymbol{\sigma} = (1-d^{+})\mathbf{P}^{+} : \bar{\boldsymbol{\sigma}} + (1-d^{-})\mathbf{P}^{-} : \bar{\boldsymbol{\sigma}} = \bar{\boldsymbol{\sigma}} - (d^{+}\mathbf{P}^{+} + d^{-}\mathbf{P}^{-}) : \bar{\boldsymbol{\sigma}} \tag{19}$$

It is then possible to obtain a final form for the constitutive law, which is a rather intuitive expression for the Cauchy stress tensor $\boldsymbol{\sigma}$ (Wu and Li, 2004)

$$\boldsymbol{\sigma} = (\mathbf{I}-\mathbf{D}) : \bar{\boldsymbol{\sigma}} = (\mathbf{I}-\mathbf{D}) : \mathbf{C}_0 : (\boldsymbol{\varepsilon} - \boldsymbol{\varepsilon}^{\mathrm{p}}) \tag{20}$$

where the fourth-order damage tensor $\mathbf{D}$ is expressed as

$$\mathbf{D} = d^{+}\mathbf{P}^{+} + d^{-}\mathbf{P}^{-} \tag{21}$$

It should be noted that Eq. (20) is the standard relation between the Cauchy stress tensor $\boldsymbol{\sigma}$ and the effective stress tensor $\bar{\boldsymbol{\sigma}}$ in CDM, according to the "equivalence strain" assumption (Lemaitre, 1985; Ju, 1989), and Eq. (21) is also coincident with Ju (1990).

From the observation of Eq. (17) the tensile and the shear DERRs Y^{+} and Y^{-}, conjugated to the corresponding damage variables, can be expressed as

$$Y^{\pm} = -\frac{\partial \psi}{\partial d^{\pm}} \tag{22}$$

Eq. (22) demonstrates that the DERRs depend on the total elastoplastic HFE potential, and not just on the elastic one as in the classical damage model of Lemaitre (1985). Accordingly, it is physically incorrect to consider the damage criteria based on the elastic DERRs alone, since disregarding the contribution of plastic strains would prevent the model from predicting the enhancement of the concrete strength under the biaxial compression (Mazars, 1985).

3. Plastic-damage model

3.1. Plastic strains

To determine the required effective stress tensor, the evolution law for the irreversible plastic strains tensor $\boldsymbol{\varepsilon}^{\mathrm{p}}$ has to be established first. Owing to the coupling between the damage evolutions and the plastic flows, the so-called "effective stress space plasticity" (Ju, 1989) should be resorted to establish the evolution laws for the plastic strains (Wu and Li, 2004)

$$\dot{\boldsymbol{\varepsilon}}^{\mathrm{p}} = \dot{\lambda}^{\mathrm{p}}\partial_{\boldsymbol{\sigma}}F^{\mathrm{p}} \tag{23a}$$

$$\dot{\boldsymbol{\kappa}} = \dot{\lambda}^{\mathrm{p}}\mathbf{H} \tag{23b}$$

$$F(\bar{\boldsymbol{\sigma}}, \boldsymbol{\kappa}) \leqslant 0, \quad \dot{\lambda}^{\mathrm{p}} \geqslant 0, \quad \dot{\lambda}^{\mathrm{p}} F(\bar{\boldsymbol{\sigma}}, \boldsymbol{\kappa}) \leqslant 0 \tag{23c}$$

where F and F^{p} are the plastic yield function and the plastic potential, respectively; $\dot{\lambda}^{\mathrm{p}}$ is the plastic flow parameter; $\mathbf{H}$ denotes the vectorial hardening function; and operator $\partial_x y = \partial y/\partial x$ is the partial differentiation operator.

Plastic potential F^{p} adopted in the present model is the Drucker–Prager function expressed as (Ortiz, 1985; Lee and Fenves, 1998)

$$F^{\mathrm{p}} = \alpha^{\mathrm{p}}\overline{I}_1 + \sqrt{2\overline{J}_2} \tag{24}$$

where $\overline{I}_1$ is the first invariant of $\bar{\boldsymbol{\sigma}}$; $\overline{J}_2$ is the second invariant of $\bar{\mathbf{s}}$, the deviatoric component of $\bar{\boldsymbol{\sigma}}$; and $\alpha^{\mathrm{p}} \geqslant 0$ is a parameter chosen to provide proper dilatancy with common range between 0.2 and 0.3 for concrete.

Combining Eqs. (23a) and (24), the evolution law for the plastic strains is obtained

$$\dot{\boldsymbol{\varepsilon}}^{\mathrm{p}} = \dot{\lambda}^{\mathrm{p}}\left(\frac{\bar{\mathbf{s}}}{\|\bar{\mathbf{s}}\|} + \alpha^{\mathrm{p}}\mathbf{1}\right) \tag{25}$$

where $\|\bar{\mathbf{s}}\| = \sqrt{\bar{\mathbf{s}} : \bar{\mathbf{s}}} = \sqrt{2\overline{J}_2}$ is the norm of $\bar{\mathbf{s}}$; $\mathbf{1}$ is the second-order identity tensor.

If one introduces the hardening parameters κ^+ and κ^- as the equivalent plastic strains under uniaxial tension and compression, respectively, with the definition

$$\kappa^+ = \int \sqrt{\dot{\varepsilon}^{\mathrm{p}}_{\max}\dot{\varepsilon}^{\mathrm{p}}_{\max}}\,\mathrm{d}t; \quad \kappa^- = \int \sqrt{\dot{\varepsilon}^{\mathrm{p}}_{\min}\dot{\varepsilon}^{\mathrm{p}}_{\min}}\,\mathrm{d}t \tag{26a, b}$$

where $\dot{\varepsilon}^{\mathrm{p}}_{\max}$ and $\dot{\varepsilon}^{\mathrm{p}}_{\min}$ are the maximum and minimum eigenvalues of the plastic strain rate tensor $\dot{\boldsymbol{\varepsilon}}^{\mathrm{p}}$, the evolution law for vector $\boldsymbol{\kappa}$ may be postulated

$$\dot{\boldsymbol{\kappa}} = \{w\dot{\kappa}^+, (1-w)\dot{\kappa}^-\}^{\mathrm{T}} = \{w\dot{\varepsilon}^{\mathrm{p}}_{\max}, -(1-w)\dot{\varepsilon}^{\mathrm{p}}_{\min}\}^{\mathrm{T}} \tag{27}$$

with w being a weight factor expressed as

$$w = \sum_{i=1}^{3}\langle\bar{\sigma}_i\rangle \Big/ \sum_{i=1}^{3}|\bar{\sigma}_i| \tag{28}$$

that is equal to one if all the eigenstresses $\bar{\sigma}_i$ are positive and equal to zero if they are all negative (Lee and Fenves, 1998). Calling for Eq. (23b), the vectorial hardening function $\mathbf{H}$ is thus derived (Wu, 2004)

$$\mathbf{H} = \begin{Bmatrix} H^+ \\ H^- \end{Bmatrix} = \begin{Bmatrix} w\partial_{\bar{\sigma}_{i,\max}}F^{\mathrm{p}} \\ -(1-w)\partial_{\bar{\sigma}_{i,\min}}F^{\mathrm{p}} \end{Bmatrix} = \mathrm{diag}[w, -(1-w)]\{\partial_{\hat{\bar{\boldsymbol{\sigma}}}}F^{\mathrm{p}}\} \tag{29}$$

where $\mathrm{diag}[\cdot]$ is a diagonal matrix; vector $\hat{\bar{\boldsymbol{\sigma}}} = \{\bar{\sigma}_{i,\max}, \bar{\sigma}_{i,\min}\}^{\mathrm{T}}$, with $\bar{\sigma}_{i,\max}$ and $\bar{\sigma}_{i,\min}$ being the maximum and minimum values of $\bar{\sigma}_i$.

Any yield function F appropriate for concrete can be adopted in Eq. (23c). Here a modified function proposed in Lubliner et al. (1989) and Lee and Fenves (1998) is adopted

$$F(\bar{\boldsymbol{\sigma}}, \boldsymbol{\kappa}) = \left(\alpha\overline{I}_1 + \sqrt{3\overline{J}_2} + \beta\langle\bar{\sigma}_{i,\max}\rangle\right) - (1-\alpha)c \tag{30}$$

with following expressions for α, β and c:

$$\alpha = (\vartheta - 1)/(2\vartheta - 1) \tag{31a}$$

$$\beta(\boldsymbol{\kappa}) = (1-\alpha)\bar{f}^-(\boldsymbol{\kappa})/\bar{f}^+(\boldsymbol{\kappa}) - (1+\alpha) \tag{31b}$$

$$c(\boldsymbol{\kappa}) = \bar{f}^-(\boldsymbol{\kappa}) \tag{31c}$$

where ϑ is the ratio between the yield strengths under equibiaxial and uniaxial compression, usually taking a value in the interval 1.10–1.20; and $\bar{f}^{+}(\boldsymbol{\kappa})$ and $\bar{f}^{-}(\boldsymbol{\kappa})$ denote evolution stresses (positive values are used here) in the effective stress space due to plastic hardening/softening under uniaxial tension and compression, respectively.

Though many hardening rules can be adopted to describe the expansion of the yield surface in the effective stress space, the following linear isotropic hardening expressions are used here for simplification:

$$\bar{f}^{\pm}(\boldsymbol{\kappa}) = \bar{f}_{\mathrm{y}}^{\pm} + E^{\mathrm{p}\pm}\kappa^{\pm} \tag{32}$$

where $\bar{f}_{\mathrm{y}}^{+}$ and $\bar{f}_{\mathrm{y}}^{-}$ are the effective yield strengths under uniaxial tension and compression, approximated as $\bar{f}_{\mathrm{y}}^{+} = f_{\mathrm{t}}$ and $\bar{f}_{\mathrm{y}}^{-} = f_{\mathrm{c}}$, with f_{t} and f_{c} being the uniaxial tensile and compressive strengths. In Eq. (32) $E^{\mathrm{p}\pm}$ are the effective plastic hardening modulus under uniaxial tension and compression relating to the elastoplastic tangent modulus $E^{\mathrm{ep}\pm}$ as follows (Simo and Hughes, 1998):

$$E^{\mathrm{ep}\pm} = \frac{E_0 E^{\mathrm{p}\pm}}{E_0 + E^{\mathrm{p}\pm}} = \left(1 - \frac{1}{1 + R_{\mathrm{E}}^{\pm}}\right) E_0 \tag{33}$$

where $R_{\mathrm{E}}^{\pm} = E^{\mathrm{p}\pm}/E_0$ denote the ratios between $E^{\mathrm{p}\pm}$ and the initial Young's modulus E_0.

Then, in rate form the relation between the effective stress and the strain tensors can be deduced by the standard procedures in classical plasticity as follows (Ju, 1989):

$$\dot{\bar{\boldsymbol{\sigma}}} = \mathbf{C}^{\mathrm{ep}} : \dot{\boldsymbol{\varepsilon}} \tag{34}$$

where $\mathbf{C}^{\mathrm{ep}}$ is the continuum effective elastoplastic tangent tensor

$$\mathbf{C}^{\mathrm{ep}} = \begin{cases} \mathbf{C}_0 & \text{if } \dot{\lambda}^{\mathrm{p}} = 0 \\ \mathbf{C}_0 - \dfrac{(\mathbf{C}_0 : \partial_{\bar{\boldsymbol{\sigma}}} F^{\mathrm{p}}) \otimes (\mathbf{C}_0 : \partial_{\bar{\boldsymbol{\sigma}}} F)}{\partial_{\bar{\boldsymbol{\sigma}}} F : \mathbf{C}_0 : \partial_{\bar{\boldsymbol{\sigma}}} F^{\mathrm{p}} - \partial_{\boldsymbol{\kappa}} F \cdot \mathbf{H}} & \text{if } \dot{\lambda}^{\mathrm{p}} > 0 \end{cases} \tag{35}$$

3.2. Plastic and elastoplastic HFE potentials

In order to clearly define concepts such as "loading", "unloading", or "reloading", damage criteria analogous to the yield criteria in plasticity should be introduced.

Since elastoplastic DERRs are the conjugated forces to the damage variables, thermodynamically consistent damage criteria should be based on $Y^{\pm}$ defined in Eq. (22). To this end, one has to determine the plastic HFE potential first.

Comparing contribution to the plastic HFE potential from plastic strains of concrete in compression, the one from tension is so much smaller that $\psi_0^{\mathrm{p}+} = 0$ can be assumed. Accordingly only the negative component $\psi_0^{\mathrm{p}-}$ is taken into consideration, in the present model through the following expression (Wu, 2004 and see also Appendix II):

$$\psi_0^{\mathrm{p}}(\boldsymbol{\kappa}) = \psi_0^{\mathrm{p}-}(\boldsymbol{\kappa}) = \frac{b}{2E_0}\left(3\bar{J}_2^{-} + \eta^{\mathrm{p}}\bar{I}_1^{-}\sqrt{3\bar{J}_2^{-}} - \frac{1}{2}\bar{I}_1^{+}\bar{I}_1^{-}\right) \tag{36}$$

where $\bar{I}_1^{\pm}$ are the first invariants of $\bar{\boldsymbol{\sigma}}^{\pm}$; $\bar{J}_2^{-}$ is the second invariant of $\bar{\mathbf{s}}^{-}$, the deviatoric tensorial components of $\bar{\boldsymbol{\sigma}}^{-}$; $\eta^{\mathrm{p}} = \sqrt{3/2}\alpha^{\mathrm{p}}$ is an alternative parameter to describe the dilatancy; and parameter b is a material property (see Appendix II for further details), devised so that the ratio between the equibiaxial and the uniaxial compressive strengths could match the usual 1.10–1.20 values (Kupfer et al., 1969).

According to the analysis of concrete micromechanics (Lemaitre, 1985), resulting mainly from internal slips on the interface between the matrix and the aggregates, plastic flow is generally controlled by the shear damage mechanism. Hence, plastic HFE potential is assumed to be a function with the form

$$\psi^{\mathrm{p}}(\boldsymbol{\kappa}, d^-) = (1-d^-)\psi_0^{\mathrm{p}}(\boldsymbol{\kappa}) \tag{37}$$

Substituting Eqs. (10)–(12) and (37) into Eq. (13), the elastoplastic HFE potential becomes

$$\psi(\boldsymbol{\varepsilon}^{\mathrm{e}}, \boldsymbol{\kappa}, d^+, d^-) = \psi^+(\boldsymbol{\varepsilon}^{\mathrm{e}}, d^+) + \psi^-(\boldsymbol{\varepsilon}^{\mathrm{e}}, \boldsymbol{\kappa}, d^-) \tag{38}$$

where

$$\psi^+(\boldsymbol{\varepsilon}^{\mathrm{e}}, d^+) = (1-d^+)\psi_0^+(\boldsymbol{\varepsilon}^{\mathrm{e}}) \tag{39a}$$

$$\psi^-(\boldsymbol{\varepsilon}^{\mathrm{e}}, \boldsymbol{\kappa}, d^-) = (1-d^-)\psi_0^-(\boldsymbol{\varepsilon}^{\mathrm{e}}, \boldsymbol{\kappa}) \tag{39b}$$

Calling for Eqs. (10) and (36), the positive and negative component of the initial elastoplastic HFE ψ_0^+ and ψ_0^- can be expressed as

$$\psi_0^+ = \psi_0^{\mathrm{e}+} = (\bar{\boldsymbol{\sigma}}^+ : \boldsymbol{\Lambda}_0 : \bar{\boldsymbol{\sigma}})/2 \tag{40a}$$

$$\psi_0^- = \psi_0^{\mathrm{e}-} + \psi_0^{\mathrm{p}-} = b_0(\alpha\bar{I}_1 + \sqrt{3\bar{J}_2})^2 \tag{40b}$$

where the introduced approximations and the expression for parameters b_0 are detailed in Appendix II.

3.3. Damage criteria and domain of linear behaviour

According to the definitions in Eq. (22), and taking Eqs. (39) into consideration, the tensile and shear DERRs are expressed as

$$Y^{\pm} = -\frac{\partial\psi^{\pm}}{\partial d^{\pm}} = \psi_0^{\pm} \tag{41}$$

With these definitions for the DERRs, the state of damage in concrete can then be characterized by means of damage criteria with the following two equivalent functional forms:

$$G^{\pm}(Y^{\pm}, r^{\pm}) = Y^{\pm} - r^{\pm} \leqslant 0 \iff \overline{G}^{\pm}(Y^{\pm}, r^{\pm}) = g^{\pm}(Y^{\pm}) - g^{\pm}(r^{\pm}) \leqslant 0 \tag{42}$$

where $r^{\pm}$ are the current damage thresholds (energy barriers), which control the size of the expanding damage surfaces. Denoting by $r_0^{\pm}$ the initial damage thresholds before any loading applied, Eq. (42) implies $r^{\pm} \geqslant r_0^{\pm}$, which states that damages are initiated when the DERRs $Y^{\pm}$ exceed the corresponding initial damage thresholds $r_0^{\pm}$.

In Eq. (42) $g^{\pm}(\cdot)$ can be any monotonically increasing scalar functions, and in the proposed model functions $\sqrt{2E_0(\cdot)}$ and $\sqrt{(\cdot)/b_0}$ are postulated for convenience, therefore the tensile and shear DERRs given in Eq. (41) can now be redefined as

$$Y^+ = \sqrt{2E_0\psi_0^+} = \sqrt{E_0(\bar{\boldsymbol{\sigma}}^+ : \boldsymbol{\Lambda}_0 : \bar{\boldsymbol{\sigma}})} \tag{43a}$$

$$Y^- = \sqrt{\psi_0^-/b_0} = \alpha\bar{I}_1 + \sqrt{3\bar{J}_2} \tag{43b}$$

Correspondingly, the initial tensile damage and shear damage thresholds are calculated as

$$r_0^+ = f_0^+; \quad r_0^- = (1-\alpha)f_0^- \tag{44}$$

where f_0^+ and f_0^- are the stresses (positive values) beyond which nonlinearity becomes visible under uniaxial tension and compression, respectively.

It should be noted that Eq. (43a) is unconditionally correct under all stress states, and Eq. (43b) holds strictly under plane stress states. And it does exist stress states under which Y^- is less than zero (e.g., under hydrostatic compression), demonstrating that the compressive consolidation mechanism could play a significant role.

Due to the above fact and the inherent shortcomings of the Drucker–Prager function, the predicted results of the present model would be somewhat conservative in triaxial compression. Under a not too high confinement compressive pressure, the shear DERR defined in Eq. (43b) can be modified to include the influence of the third invariant of $\bar{\boldsymbol{\sigma}}$, namely through equation (Li and Wu, 2004)

$$Y^- = \alpha \bar{I}_1 + \sqrt{3\bar{J}_2} - \gamma\langle -\bar{\sigma}_{i,\max}\rangle \tag{45}$$

with

$$\gamma = 3(1-K_c)/(2K_c-1) \tag{46}$$

where K_c, assumed as a constant (Lubliner et al., 1989), denotes the ratio of corresponding values of $\sqrt{\bar{J}_2}$ under tensile meridian and compressive meridian stress states for any given value of hydrostatic pressure $\bar{I}_1$. A value of $K_c = 2/3$ typical for concrete, gives $\gamma = 3.0$, which is adopted here.

Note that in Eq. (45) the influence of coefficient γ disappears in stress states other than triaxial compression, namely when $\bar{\sigma}_{i,\max} \geqslant 0$. Therefore, Eq. (45) can be viewed as a minor modification of Eq. (43b) to improve the predictive capability of the proposed model under stress state when the later does not hold.

Under biaxial stress states the damage criteria defined through Eqs. (42)–(45) lead to the domain of linear behaviour shown in Fig. 1, which agrees rather well with the experimental results from Kupfer et al. (1969).

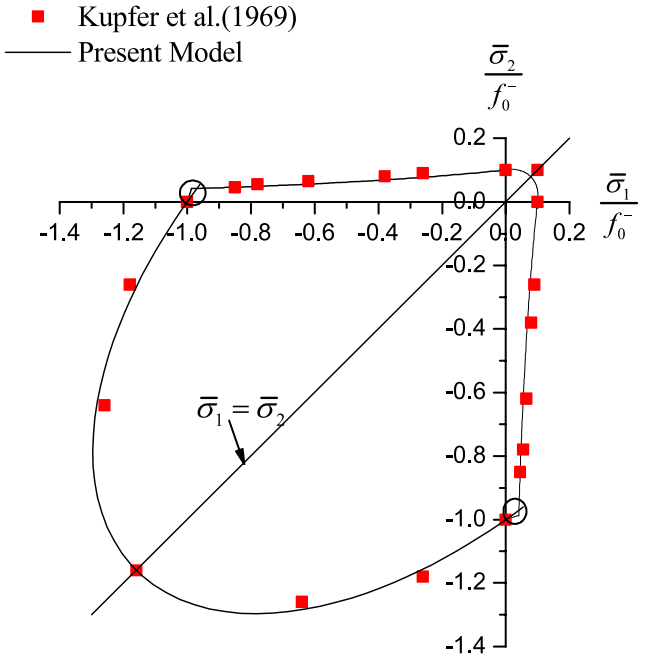

Fig. 1. Domain of linear behaviour of concrete under biaxial stresses.

3.4. Characterization of damage

To describe the growth of microcracks and the evolution of the damage surfaces, it is necessary to specify the evolution laws for the damage variables $d^{\pm}$ and the corresponding damage thresholds $r^{\pm}$. Analogous to the normality rule in classical plasticity, the evolution laws for the damage variables can be defined by applying it to the damage criteria prescribed in Eq. (42)

$$\dot{d}^{\pm} = \dot{\lambda}^{d\pm} \frac{\partial g^{\pm}(Y^{\pm})}{\partial Y^{\pm}}; \quad \dot{\lambda}^{d\pm} = \dot{r}^{\pm} \tag{47a, b}$$

where $\dot{\lambda}^{d\pm}$ are damage consistency parameters.

In compacted form loading or unloading can be expressed through the Kuhn–Tucker relations

$$\dot{\lambda}^{d\pm} \geqslant 0; \quad \overline{G}^{\pm}(Y^{\pm}, r^{\pm}) \leqslant 0; \quad \dot{\lambda}^{d\pm}\overline{G}^{\pm}(Y^{\pm}, r^{\pm}) = 0 \tag{48a, b, c}$$

Calling for the damage consistency condition, one obtains

$$\overline{G}^{\pm}(Y^{\pm}, r^{\pm}) = \dot{\overline{G}}^{\pm}(Y^{\pm}, r^{\pm}) = 0 \tag{49}$$

which yields

$$r^{\pm} = Y^{\pm}; \quad \dot{\lambda}^{d\pm} = \dot{r}^{\pm} = \dot{Y}^{\pm} \geqslant 0 \tag{50}$$

So for a generic instant n thresholds $r^{\pm}$ are given by (Ju, 1989; Faria et al., 1998)

$$r^{\pm} = \max\left\{ r_0^{\pm}, \max_{\tau\in[0,n]} Y_{\tau}^{\pm} \right\} \tag{51}$$

Introducing Eq. (50) into Eq. (47a), the evolution laws for the damage variables during loading are expressed as

$$\dot{d}^{\pm} = \dot{r}^{\pm} \frac{\partial g^{\pm}(r^{\pm})}{\partial r^{\pm}} = \dot{g}^{\pm}(r^{\pm}) \tag{52}$$

Performing a trivial integration and accounting for the initial conditions $d^{\pm}(r_0^{\pm}) = 0$, one obtains

$$d^{\pm} = g^{\pm}(r^{\pm}) \tag{53}$$

Usually concrete under one-dimensional tension is assumed to behave elastically until the stress reaches the tensile strength $f_t = f_0^+$, hardening is disregarded and the following function is adopted for damage variable d^+:

$$d^+ = g^+ = 1 - \frac{r_0^+}{r^+}\left\{ (1 - A^+) + A^+ \exp\left[B^+ \left(1 - \frac{r^+}{r_0^+} \right) \right] \right\} \tag{54}$$

where parameters A^+ and B^+ are related to the percentage of steel ρ_s in reinforced concrete, which in accordance with experimental tests can be expressed as following (Stevens et al., 1991):

$$A^+ = 1 - c_s\rho_s/d_b \tag{55a}$$

$$B^+ = (270/\sqrt{A^+})f_0^+/E_0 \leqslant 1000 f_0^+/E_0 \tag{55b}$$

in which d_b is the rebar diameter (in mm); and c_s has the dimension of length, and generally takes the value of 75 mm.

Eq. (54) actually describes the overall tension-stiffening effect due to the interaction between steel rebars and concrete. In plain concrete $A^+ = 1.0$ is obtained from Eq. (55a), thus Eq. (54) reduces to the function first proposed by Oliver et al. (1990)

$$d^+ = g^+ = 1 - \frac{r_0^+}{r^+} \exp\left[B^+\left(1 - \frac{r^+}{r_0^+}\right)\right] \tag{56}$$

To reduce sensitivity in the analysis of plain concrete as regards to the refinement of the finite element meshes, parameter B^+ involved in Eq. (56) should be computed so as to satisfy the requirement of mesh objectivity (see Oliver et al., 1990)

$$B^+ = \left[\frac{G_f E_0}{l_{\mathrm{ch}}(f_0^+)^2} - \frac{1}{2}\right]^{-1} \geqslant 0 \tag{57}$$

where l_{ch} is the "geometrical" characteristic length of finite element mesh.

To allow reproducing the hardening of concrete in compression, as well as the softening which characterizes the post-peak behaviour, the following evolution for damage variable d^- is adopted (Mazars, 1985; Faria et al., 1998):

$$d^- = g^- = 1 - \left\{\frac{r_0^-}{r^-}(1 - A^-) + A^- \exp\left[B^-\left(1 - \frac{r^-}{r_0^-}\right)\right]\right\} \tag{58}$$

where parameters A^- and B^- may be determined by imposing the simulation curve to fit the one obtained from a one-dimensional experimental test.

Correspondingly, from Eqs. (52), (54) and (58) the evolution laws for $d^\pm$ are expressed as

$$\dot{d}^\pm = \dot{r}^\pm h^\pm \geqslant 0 \tag{59}$$

where $h^\pm$ are the following hardening/softening functions:

$$h^+ = \frac{\partial g^+(r^+)}{\partial r^+} = (1 - A^+)\frac{r_0^+}{(r^+)^2} + A^+ \frac{B^+ r^+ + r_0^+}{(r^+)^2} \exp\left[B^+\left(1 - \frac{r^+}{r_0^+}\right)\right] \tag{60a}$$

$$h^- = \frac{\partial g^-(r^-)}{\partial r^-} = (1 - A^-)\frac{r_0^-}{(r^-)^2} + \frac{A^- B^-}{r_0^-} \exp\left[B^-\left(1 - \frac{r^-}{r_0^-}\right)\right] \tag{60b}$$

4. Computational aspects

4.1. Numerical algorithm

To explore the numerical implementation algorithm for the proposed plastic-damage model, the constitutive law in Eq. (20) has to be differentiated with respect to time, leading to

$$\dot{\boldsymbol{\sigma}} = (\mathbf{I} - \boldsymbol{\omega}) : \mathbf{C}_0 : (\dot{\boldsymbol{\varepsilon}} - \dot{\boldsymbol{\varepsilon}}^{\mathrm{p}}) - (\bar{\boldsymbol{\sigma}}^+ \dot{d}^+ + \bar{\boldsymbol{\sigma}}^- \dot{d}^-) \tag{61}$$

with the symmetric fourth-order tensors $\boldsymbol{\omega}$ being

$$\boldsymbol{\omega} = d^+ \mathbf{Q}^+ + d^- \mathbf{Q}^- \tag{62}$$

According to the concept of operator split (Ju, 1989; Simo and Hughes, 1998), Eq. (61) can be decomposed into elastic, plastic and damage parts, leading to the corresponding numerical algorithm including elastic-predictor, plastic-corrector and damage-corrector steps, as established in Box 1 with Eqs. (63).

Box 1. Numerical algorithm (operator split)

Elastic-predictor (63a)	Plastic-corrector (63b)	Damage-corrector (63c)
$\dot{\boldsymbol{\varepsilon}} = \nabla^s \dot{\mathbf{u}}(t)$ $\dot{\boldsymbol{\varepsilon}}^{\mathrm{p}} = 0$	$\dot{\boldsymbol{\varepsilon}} = 0$ $\dot{\boldsymbol{\varepsilon}}^{\mathrm{p}} = \begin{cases} \dot{\lambda}^{\mathrm{p}} \partial_{\bar{\boldsymbol{\sigma}}} F^{\mathrm{p}} & \text{if } F = \dot{F} = 0 \\ 0 & \text{otherwise} \end{cases}$	$\dot{\boldsymbol{\varepsilon}} = 0$ $\dot{\boldsymbol{\varepsilon}}^{\mathrm{p}} = 0$
$\dot{\boldsymbol{\kappa}} = 0$ $\dot{\bar{\boldsymbol{\sigma}}} = \mathbf{C}_0 : \dot{\boldsymbol{\varepsilon}}$	$\dot{\boldsymbol{\kappa}} = \dot{\lambda}^{\mathrm{p}} \mathbf{H}$ $\dot{\bar{\boldsymbol{\sigma}}} = -\mathbf{C}_0 : \dot{\boldsymbol{\varepsilon}}^{\mathrm{p}}$	$\dot{\boldsymbol{\kappa}} = 0$ $\dot{\bar{\boldsymbol{\sigma}}} = 0$
$\dot{d}^{\pm} = 0$	$\dot{d}^{\pm} = 0$	$\dot{d}^{\pm} = \begin{cases} \dot{r}^{\pm} h^{\pm} & \text{if } \overline{G}^{\pm} = \dot{\overline{G}}^{\pm} = 0 \\ 0 & \text{otherwise} \end{cases}$
$\dot{r}^{\pm} = 0$	$\dot{r}^{\pm} = 0$	$\dot{r}^{\pm} = \begin{cases} \dot{Y}^{\pm} & \text{if } G^{\pm} = \dot{\overline{G}}^{\pm} = 0 \\ 0 & \text{otherwise} \end{cases}$
$\dot{\boldsymbol{\sigma}} = (\mathbf{I} - \boldsymbol{\omega}) : \mathbf{C}_0 : \dot{\boldsymbol{\varepsilon}}$	$\dot{\boldsymbol{\sigma}} = -(\mathbf{I} - \boldsymbol{\omega}) \mathbf{C}_0 : \dot{\boldsymbol{\varepsilon}}^{\mathrm{p}}$	$\dot{\boldsymbol{\sigma}} = -(\bar{\boldsymbol{\sigma}}^{+} \dot{d}^{+} + \bar{\boldsymbol{\sigma}}^{-} \dot{d}^{-})$

It is noted that during the elastic-predictor and the plastic-corrector steps the damage variables are fixed, so Eqs. (63a) and (63b) are decoupled with the damage part (63c), constituting a standard elastoplastic problem in the effective stress space. Regarding to the plastic yield function Eq. (30) adopted, the spectral decomposition form (Lee and Fenves, 2002) of return mapping algorithm (Simo and Hughes, 1998) is modified and improved to update the effective stress tensor $\bar{\boldsymbol{\sigma}}$.

Once $\bar{\boldsymbol{\sigma}}$ is updated in the elastic-predictor and plastic-corrector steps, the damage variables $d^{\pm}$ and the Cauchy stress $\boldsymbol{\sigma}$ can thus be updated correspondingly in the damage-corrector step.

4.2. Algorithmic consistent tangent modulus

In the nonlinear finite element analysis, especially when post-peak behaviour is expected, the full Newton–Raphson method is usually adopted in the global iteration; hence, algorithmic consistent tangent modulus is required. According to Eq. (61), the total differential of Eq. (20) leads to

$$\mathrm{d}\boldsymbol{\sigma} = (\mathbf{I} - \boldsymbol{\omega}) : \mathrm{d}\bar{\boldsymbol{\sigma}} - [\bar{\boldsymbol{\sigma}}^{+} \mathrm{d}(d^{+}) + \bar{\boldsymbol{\sigma}}^{-} \mathrm{d}(d^{-})] \tag{64}$$

Calling for Eqs. (43a), (45) and (59); and taking Eq. (50b) into consideration, the differentials of damage variables in Eq. (64) are

$$\mathrm{d}(d^{+}) = h^{+} \mathrm{d}(r^{+}) = h^{+} \frac{E_0}{2Y^{+}} (\bar{\boldsymbol{\sigma}} : \boldsymbol{\Lambda}_0 : \mathbf{Q}^{+} + \bar{\boldsymbol{\sigma}}^{+} : \boldsymbol{\Lambda}_0) : \mathrm{d}\bar{\boldsymbol{\sigma}} \tag{65a}$$

$$\mathrm{d}(d^{-}) = h^{-} \mathrm{d}(r^{-}) = h^{-} \left(\alpha \mathbf{1} + \frac{3}{2\sqrt{3\overline{J}_2}} \bar{\mathbf{s}} + \gamma H(-\bar{\sigma}_{i,\max}) \mathbf{p}_{ii,\max} \right) : \mathrm{d}\bar{\boldsymbol{\sigma}} \tag{65b}$$

with $\mathbf{p}_{ii,\max}$ being the tensor $\mathbf{p}_{ij}$ associated to $\bar{\sigma}_{i,\max}$. Then it can be easily concluded that

$$\bar{\boldsymbol{\sigma}}^{+} \mathrm{d}(d^{+}) = \mathbf{R}^{+} : \mathrm{d}\bar{\boldsymbol{\sigma}}; \quad \bar{\boldsymbol{\sigma}}^{-} \mathrm{d}(d^{-}) = \mathbf{R}^{-} : \mathrm{d}\bar{\boldsymbol{\sigma}} \tag{66}$$

where

$$\mathbf{R}^{+} = h^{+} \frac{E_0}{2Y^{+}} [(\bar{\boldsymbol{\sigma}}^{+} \otimes \bar{\boldsymbol{\sigma}}) : \boldsymbol{\Lambda}_0 : \mathbf{Q}^{+} + (\bar{\boldsymbol{\sigma}}^{+} \otimes \bar{\boldsymbol{\sigma}}^{+}) : \boldsymbol{\Lambda}_0] \tag{67a}$$

$$\mathbf{R}^{-} = h^{-} \left[\bar{\boldsymbol{\sigma}}^{-} \otimes \left(\alpha \mathbf{1} + \frac{3}{2\sqrt{3\overline{J}_2}} \bar{\mathbf{s}} + \gamma H(-\bar{\sigma}_{i,\max}) \mathbf{p}_{ii,\max} \right) \right] \tag{67b}$$

By introducing Eqs. (66) into Eq. (64), one gets

$$d\boldsymbol{\sigma} = (\mathbf{I} - \boldsymbol{\omega} - \mathbf{R}) : d\bar{\boldsymbol{\sigma}} = \left[(\mathbf{I} - \boldsymbol{\omega} - \mathbf{R}) : \overline{\mathbf{C}}^{\mathrm{alg}}\right] : d\boldsymbol{\varepsilon} = \mathbf{C}^{\mathrm{alg}} : d\boldsymbol{\varepsilon} \tag{68}$$

with the algorithmic consistent tangent modulus $\mathbf{C}^{\mathrm{alg}}$ expressed as

$$\mathbf{C}^{\mathrm{alg}} = (\mathbf{I} - \boldsymbol{\omega} - \mathbf{R}) : \overline{\mathbf{C}}^{\mathrm{alg}} \tag{69}$$

where $\mathbf{R} = \mathbf{R}^{+} + \mathbf{R}^{-}$; and $\overline{\mathbf{C}}^{\mathrm{alg}}$ denotes the usual effective elastoplastic tangent modulus consistent with the algorithm for updating the effective stress in the previous mentioned elastic-predictor and plastic-corrector steps, satisfying

$$d\bar{\boldsymbol{\sigma}}_{n+1} = \overline{\mathbf{C}}^{\mathrm{alg}} : d\boldsymbol{\varepsilon}_{n+1} \tag{70}$$

with the following expression (Wu, 2004):

$$\overline{\mathbf{C}}^{\mathrm{alg}} = \left(\Lambda_0 + \partial_{\bar{\boldsymbol{\sigma}}} F^{\mathrm{p}} \otimes \frac{d\Delta\lambda^{\mathrm{p}}}{d\bar{\boldsymbol{\sigma}}_{n+1}} + \Delta\lambda^{\mathrm{p}} \partial^2_{\bar{\boldsymbol{\sigma}}} F^{\mathrm{p}}\right)^{-1} \tag{71}$$

where

$$\frac{d\Delta\lambda^{\mathrm{p}}}{d\bar{\boldsymbol{\sigma}}_{n+1}} = -\frac{\partial_{\bar{\boldsymbol{\sigma}}} F}{\partial_{\boldsymbol{\kappa}} F \cdot \left(\mathbf{H} + \Delta\lambda^{\mathrm{p}} \partial_{\hat{\bar{\boldsymbol{\sigma}}}} \mathbf{H} \cdot \partial_{\Delta\lambda^{\mathrm{p}}} \hat{\bar{\boldsymbol{\sigma}}}\right)} \tag{72}$$

5. Applications

To illustrate the applicability and effectiveness of the proposed model, several numerical examples of various loading conditions of concrete are presented in this section. The results obtained by the suggested model are compared with corresponding experimental results to learn its performance. For all cases, unless otherwise specified, Poisson's ratio is 0.20; the equibiaxial to uniaxial compressive strength ratio ϑ is 1.16, and the dilatancy parameter α^{p} is chosen as 0.20.

5.1. Monotonic uniaxial tensile tests

The experimental results from two typical monotonic uniaxial tensile tests (Geopalaeratnam and Shah, 1985; Zhang, 2001) are employed for the comparison purpose. The material properties used in the two test were: (1) for Geopalaeratnam and Shah's test, $E_0 = 3.1 \times 10^4$ MPa, $f_0^{+} = 3.48$ MPa, $G_{\mathrm{f}} = 100$ N/m; (2) for Zhang's test, $E_0 = 3.8 \times 10^4$ MPa, $f_0^{+} = 3.40$ MPa, $G_{\mathrm{f}} = 70$ N/m. Fig. 2 compares the predicted stress–strain curves from the proposed model with those obtained from the experimental tests. For both tests, as it can be observed from Fig. 2, predictions from the numerical model agree well with the experimental data, especially for the post-peak nonlinear softening branches.

5.2. Monotonic uniaxial compressive tests

The model ability to reproduce the concrete behaviour under monotonic uniaxial compression can be checked in Fig. 3, where two types of experimental results taken from Karson and Jirsa (1969) and Zhang (2001) are plotted against the numerical predictions. The material properties adopted in the simulations were: for the former one, $E_0 = 3.17 \times 10^4$ MPa, $f_0^{+} = 3.0$ MPa and $f_0^{-} = 10.2$ MPa; and for the latter one, $E_0 = 3.8 \times 10^4$ MPa, $f_0^{+} = 3.40$ MPa and $f_0^{-} = 43.0$ MPa. As shown in Fig. 3, either in the hardening

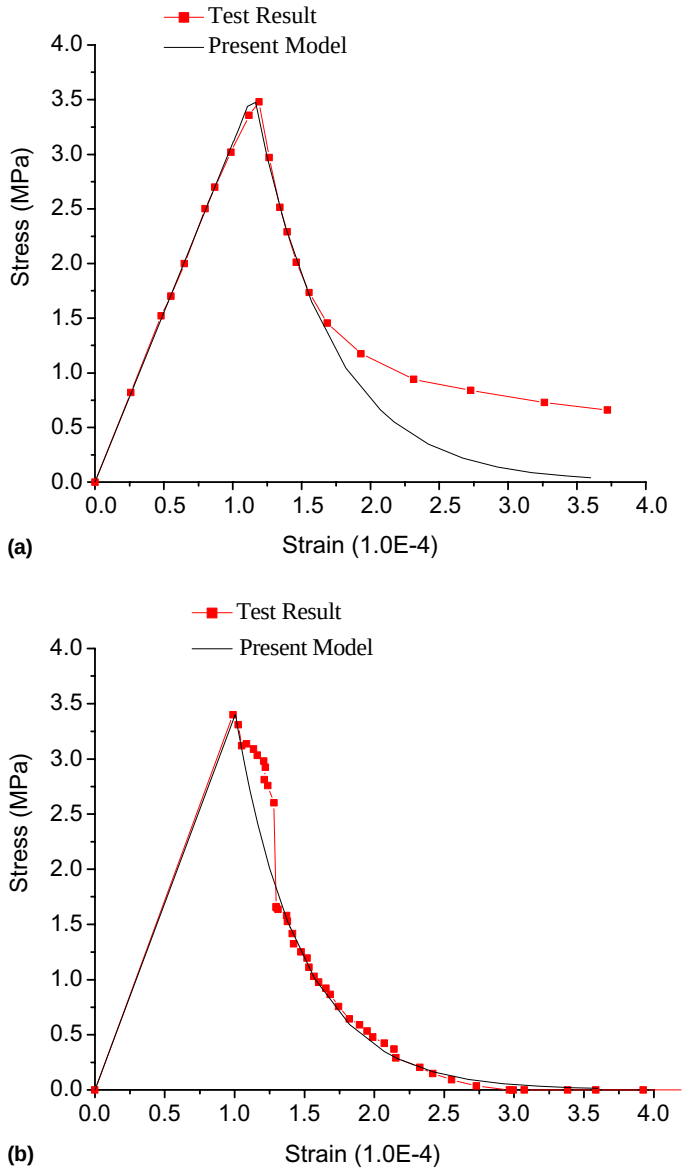

Fig. 2. Monotonic uniaxial tensile tests: (a) Geopalaeratnam and Shah (1985); (b) Zhang (2001).

or in the softening regimes, the overall nonlinear performances numerically predicted and the experimental obtained stress–strain curves are rather close.

5.3. Monotonic biaxial stress test

The proposed model is also validated with the results under biaxial compression ($\sigma_3 = 0$) reported in Kupfer et al. (1969). The material properties adopted in the simulation were: $E_0 = 3.1 \times 10^4$ MPa, $f_0^+ = 3.0$ MPa, $f_0^- = 15.0$ MPa, $G_f = 75$ N/m. For specimens under load conditions $\sigma_2/\sigma_1 = -1/0$,

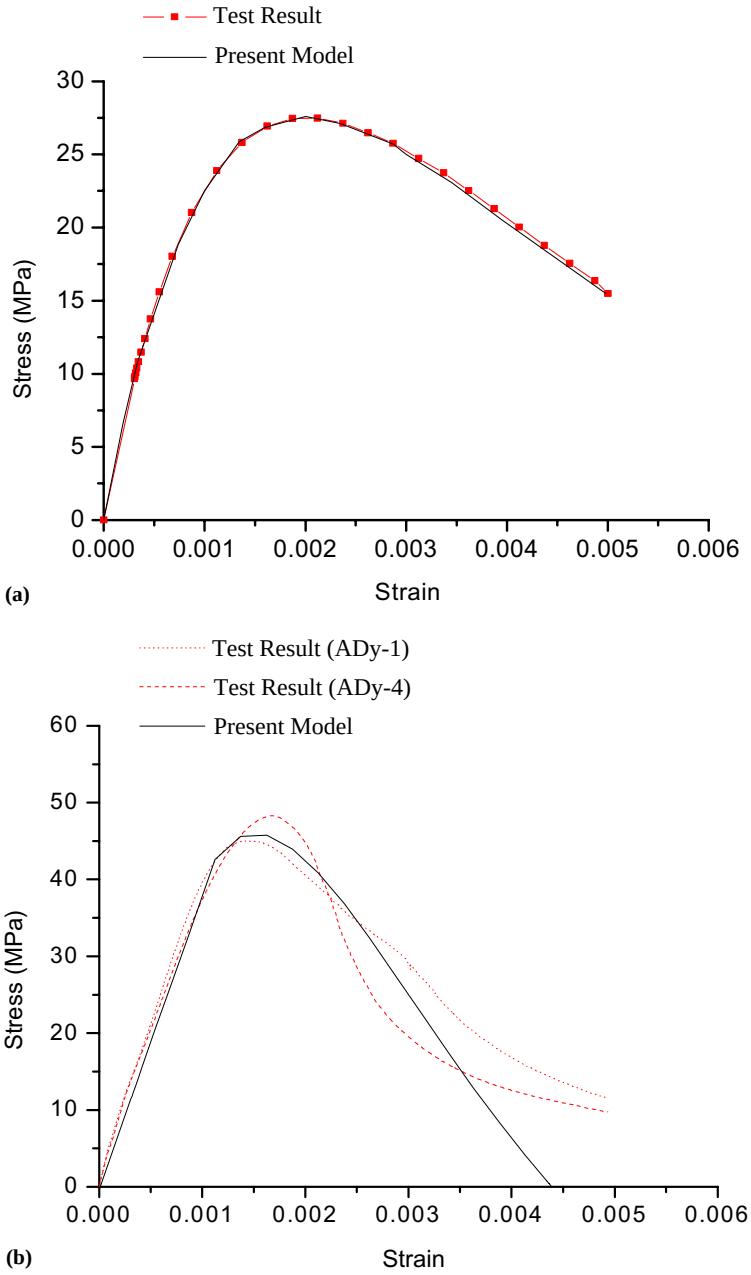

Fig. 3. Monotonic uniaxial compressive tests: (a) Karson and Jirsa (1969); (b) Zhang (2001).

$\sigma_2/\sigma_1 = -1/-1$ and $\sigma_2/\sigma_1 = -1/-0.52$, the predicted stress–strain curves illustrated in Fig. 4a–c agree well with the experimental ones, capturing the overall experimental behaviour.

To illustrate the capability of the proposed model for predicting the nonlinear behaviour of concrete under other biaxial stress states, using the same material properties as above, the numerical biaxial strength envelope is reproduced in Fig. 4d as well, which is found to be almost coincident with the experimental one

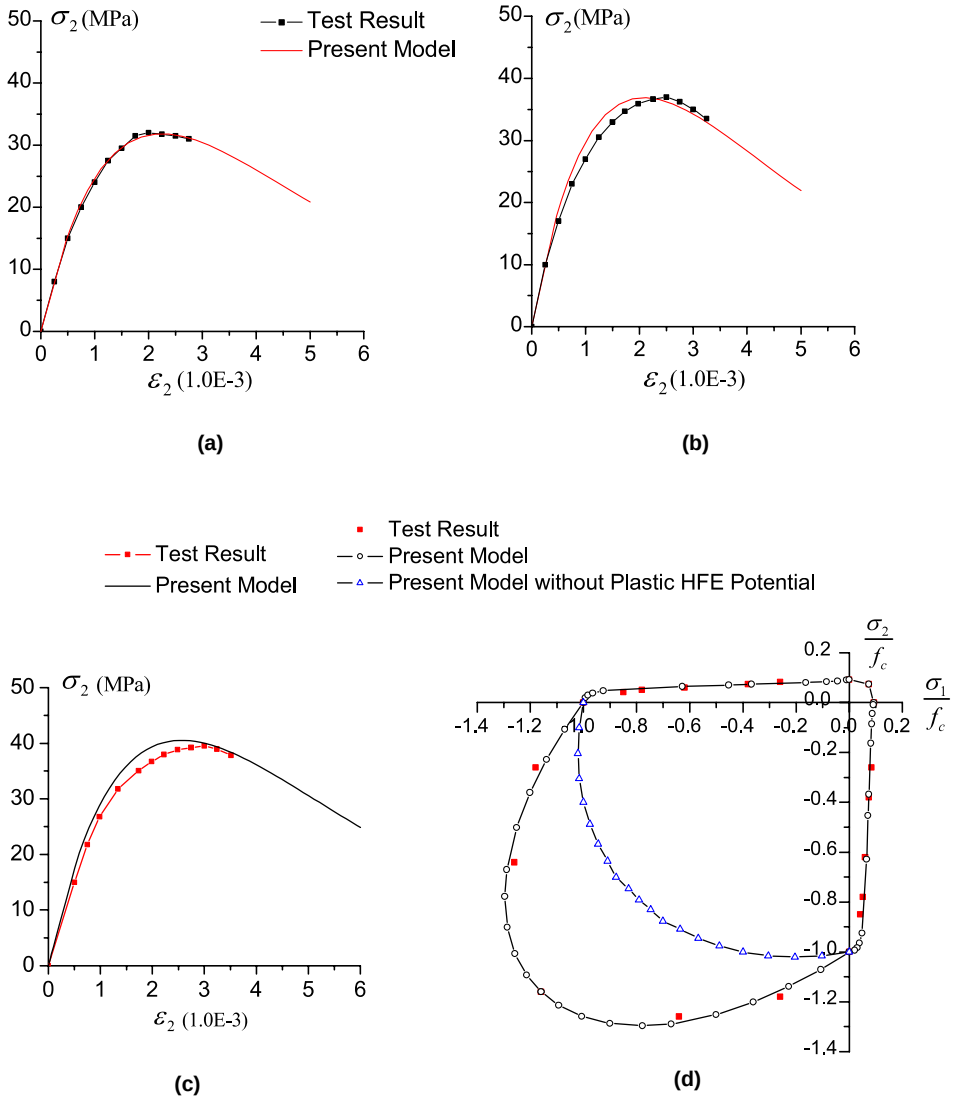

Fig. 4. Monotonic biaxial compressive tests (Kupfer et al., 1969): (a) $\sigma_2/\sigma_1 = -1/0$; (b) $\sigma_2/\sigma_1 = -1/-1$; (c) $\sigma_2/\sigma_1 = -1/-0.52$; (d) strength envelope under biaxial stresses.

from Kupfer et al. (1969). The predicted envelope without considering the contribution of the plastic HFE potential is also provided in Fig. 4d, which reproduces the same conservative results as those of Mazars (1985). As clearly perceptible in Fig. 4d, another important attribute of the present model is its ability to predict not only the enhancement of concrete strength under biaxial compression, but also the reduction on the compressive strength induced by orthogonal tensile cracking under tension–compression stress states.

5.4. Concrete under 3D compression

To check the application of the proposed model to concrete in compression under confinement, Fig. 5 compares the numerical predictions with the experimental results obtained by Green and Swanson (1973).

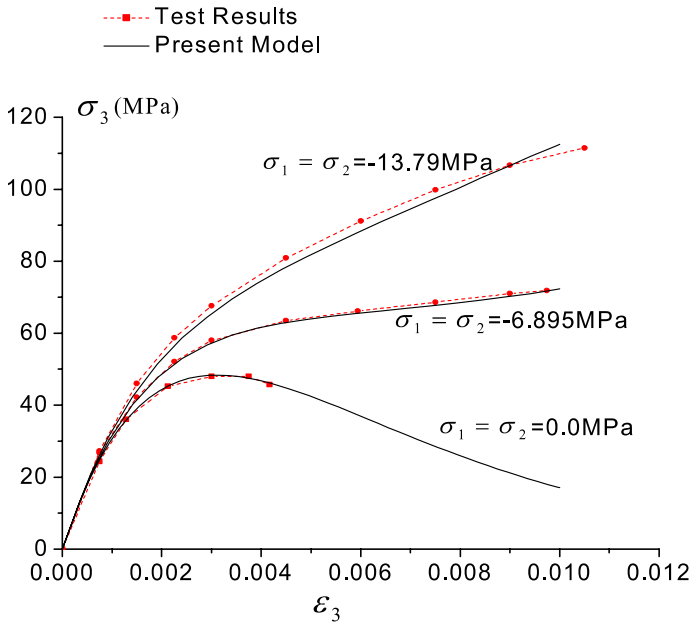

Fig. 5. 3D compression test (Green and Swanson, 1973).

To fit the uniaxial compressive stress–strain curve also reported in Fig. 5, the material properties adopted in the simulation were: $E_0 = 3.7 \times 10^4$ MPa, $f_0^+ = 4.0$ MPa, $f_0^- = 15.0$ MPa. The numerical predictions of specimens under three sets of confining stresses, namely, $\sigma_1 = \sigma_2 = 0.0$ MPa, $\sigma_1 = \sigma_2 = -6.895$ MPa and $\sigma_1 = \sigma_2 = -13.79$ MPa, are reproduced in Fig. 5. It can be clearly seen that the enhancement of strength and ductility due to the compressive confinement, as well as the overall stress–strain experimental curves, are satisfactorily predicted by the proposed model.

5.5. Cyclic uniaxial tests

In Fig. 6 the cyclic uniaxial tensile test of Taylor (1992) and the cyclic compressive test of Karson and Jirsa (1969) are reproduced numerically to demonstrate the capability of the proposed model under cyclic load conditions. The following properties were adopted: for Taylor's simulation, $E_0 = 3.17 \times 10^4$ MPa, $f_0^+ = 3.50$ MPa, $G_f = 24$ N/m; and for Karsan and Jirsa's one, $E_0 = 3.0 \times 10^4$ MPa, $f_0^- = 15.0$ MPa. As shown in Fig. 6, under both tension and compression, the experimentally observed strength softening and stiffness degrading, as well as the irreversible strains upon unloading, are well reproduced by the proposed model.

5.6. Concrete dam under earthquake motions

To further illustrate the capability of the proposed model, the Koyna dam subjected to the recorded transverse and vertical components of the ground accelerations during the earthquake motions in 1967, extensively studied by other investigators (Chopra and Chakrabarti, 1973; Bhattacharjee and Leeger, 1993; Ghrib and Tinawi, 1995; Cervera et al., 1996; and Lee and Fenves, 1998; etc.), is analyzed here.

Following the work of above investigators, the dam-foundation interactions was ignored assuming a rigid foundation, and a finite element mesh consisting of 760 4-node plane stress elements with 2×2 Gauss integration was adopted to model the dam. The dam-reservoir dynamic interactions were modeled using a

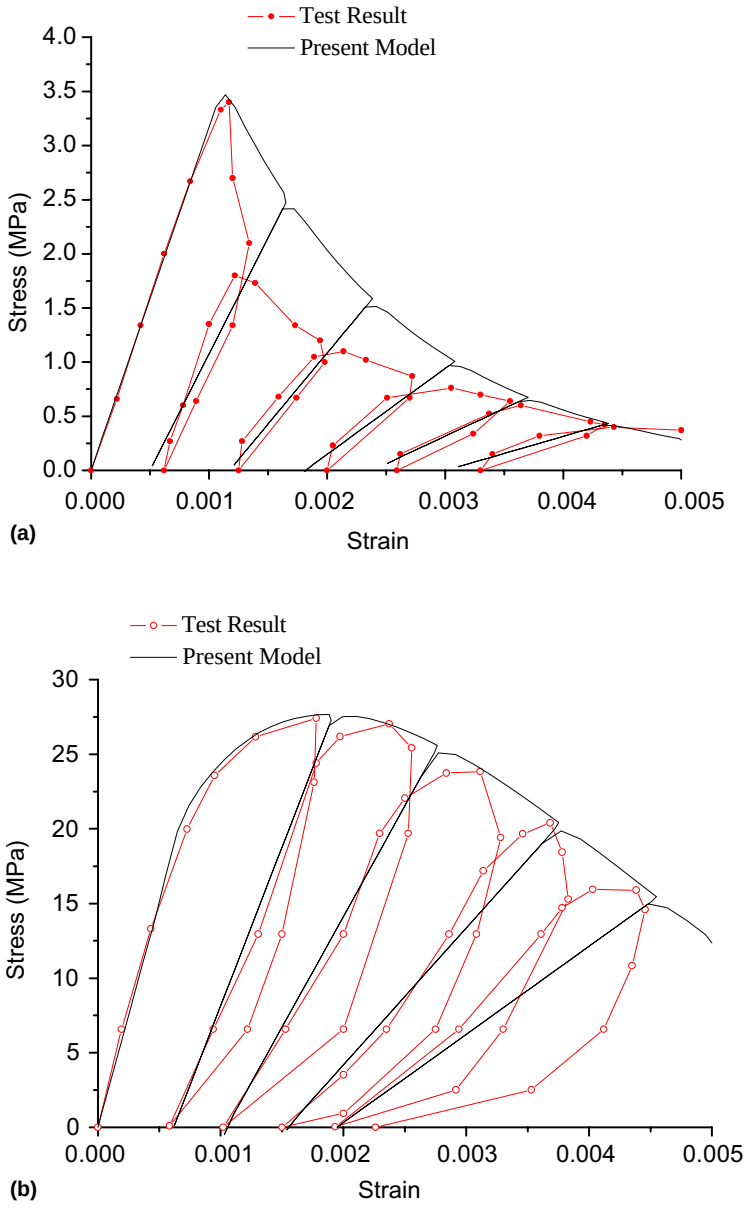

Fig. 6. Cyclic uniaxial tests: (a) cyclic uniaxial tension test (Taylor, 1992); (b) cyclic uniaxial compressive test (Karson and Jirsa, 1969).

2-node element by the added mass technique of Westergaard (1933). A Rayleigh stiffness-proportional damping factor was assumed to provide a 3% fraction of the critical damping for the first mode of vibration of the dam. The generally used Hilber–Hughes–Taylor HHT-α method was adopted to integrate the dynamic equation of motion. The material properties adopted in the simulation were: density $\rho_0 = 2643$ kg/m^3, $E_0 = 31027$ MPa, $f_t = f_0^+ = 2.9$ MPa, $f_c = 24.1$ MPa, $G_f = 200$ N/m.

The predicted results of the horizontal displacements at the left corner of the dam crest are shown in Fig. 7a and b (the positive values represent the displacement towards downstream), which agree well with those by Lee and Fenves (1998). The evolution of tensile damage and the damage patterns predicted by the

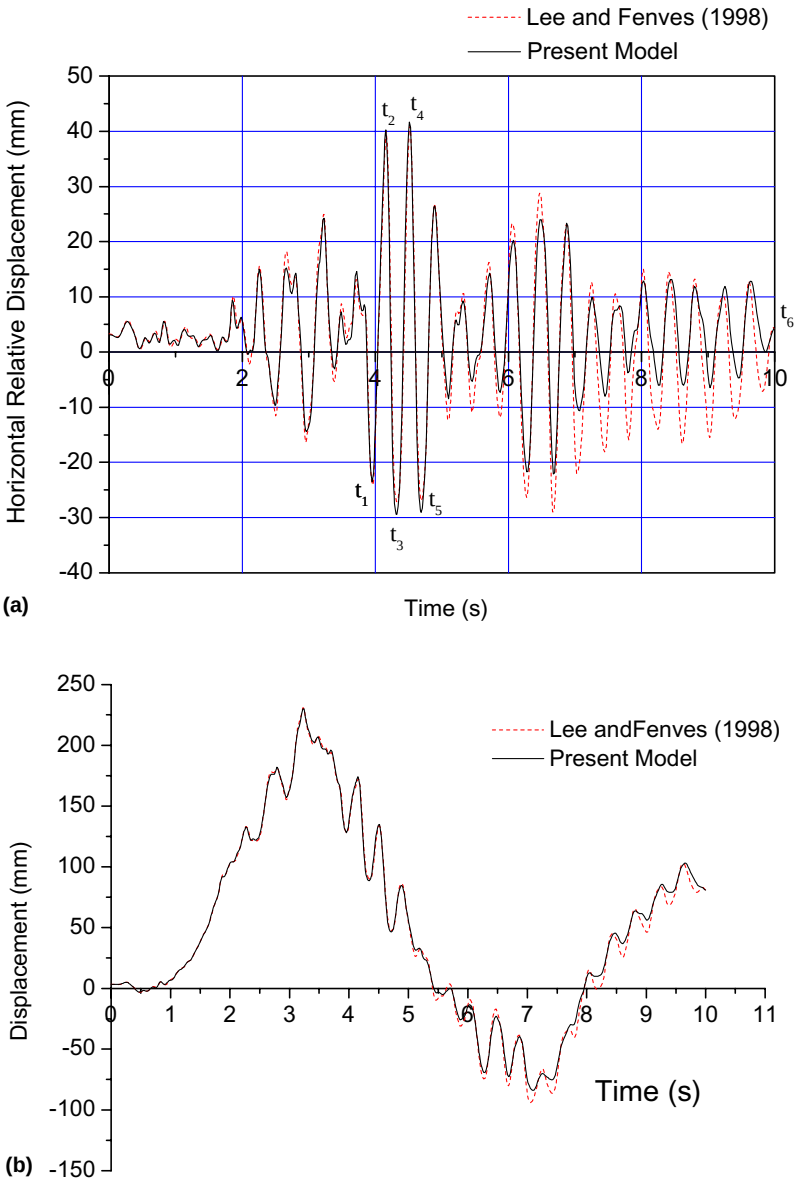

Fig. 7. Koyna dam under earthquake motions: (a) horizontal crest displacement relative to ground; (b) spatial horizontal crest displacement.

proposed model (Wu, 2004) are also in fair agreement with the observed damages reported by other investigators (Bhattacharjee and Leeger, 1993; Lee and Fenves, 1998).

5.7. Reinforced concrete slab

A square slab experimentally tested by McNeice (1967), supported at the four corners and loaded by a point load at its center, is to be simulated herein. The slab was reinforced in the two directions at 75% of its

depth, and the reinforcement ratio was 0.85% in each direction. The material properties for the concrete were: $E_0 = 28.6$ GPa; $v_0 = 0.15$; $f_0^+ = 3.17$ MPa, $f_0^- = 10.68$ MPa. For steel rebars, the material properties were: Young's modulus equal to 200 GPa and yield strength equal to 345 MPa (an elastic-perfectly plastic behaviour was assumed). One quarter of the slab is modeled regarding to the geometry symmetries. A 3×3 mesh of 8-node shell elements is used for modeling the concrete where the proposed model was enforced,

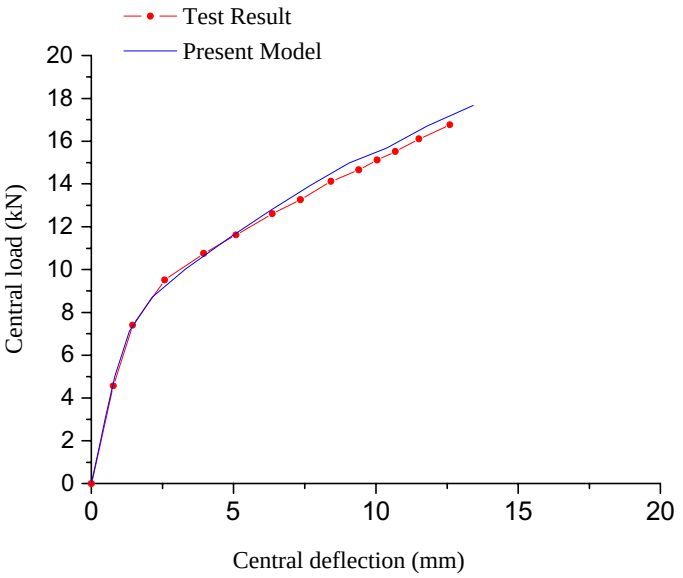

Fig. 8. RC slab test (McNeice, 1967).

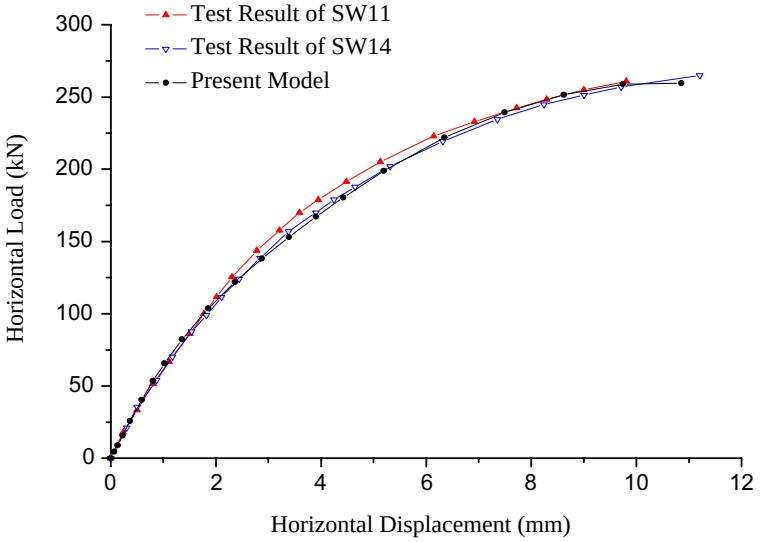

Fig. 9. RC shearwall tests (Lefas et al., 1990).

and the two-way reinforcement was modeled using smeared rebar layers, each one with an appropriate thickness of the exact cross-sectional area of reinforcement.

The comparison between the experimental result and the numerical simulation is presented in Fig. 8 in terms of a curve representing the central load versus the central deflection of the slab. It can be clearly seen that the predicted results of the proposed model, namely the cracking and the ultimate loads, as well as the entire load–deflection curve, fit rather well the experimental ones.

5.8. Reinforced concrete shearwalls

The proposed model was also used to simulate the nonlinear performances of 13 large-scale reinforced concrete shearwalls, tested by Lefas et al. (1990) under various axial and monotonically increasing horizontal forces. The experiment consisted of two types of geometries: type 1 with a height/width ratio equal to

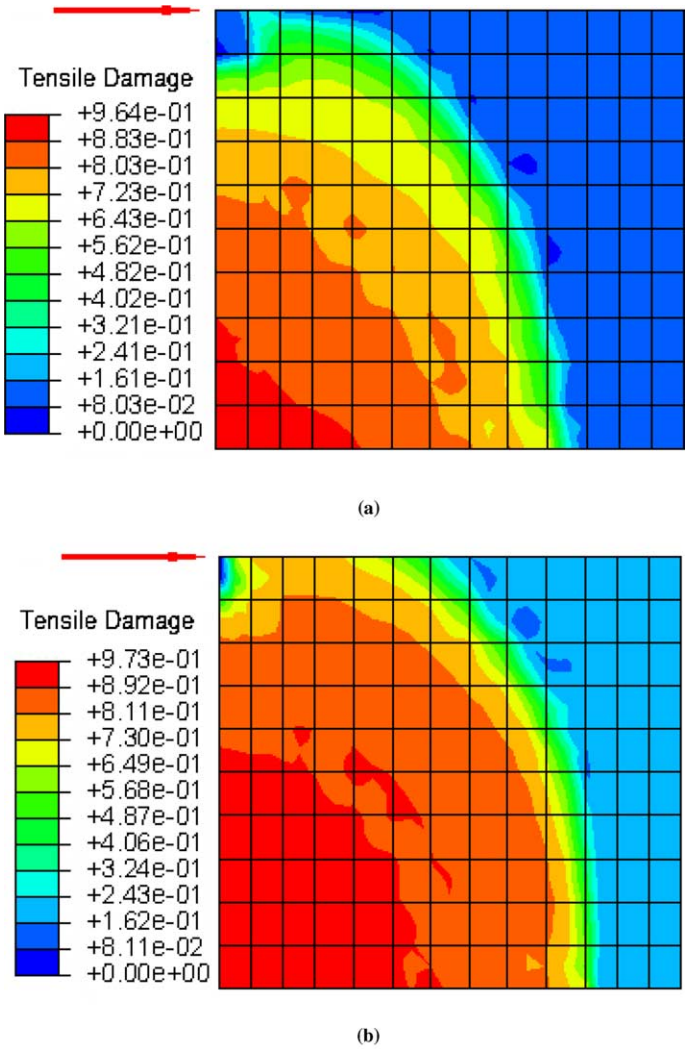

Fig. 10. Distribution of tensile damage in shearwall SW11—(a) horizontal force: 122.0 kN; (b) horizontal force: 153.1 kN.

Table 1
Peak horizontal forces and corresponding displacements for the shearwalls

Wall	$F_{u,\text{test}}$ (kN)	$F_{u,\text{model}}$ (kN)	$F_{u,\text{model}}/F_{u,\text{test}}$	$U_{u,\text{test}}$ (mm)	$U_{u,\text{model}}$ (mm)	$U_{u,\text{model}}/U_{u,\text{test}}$
SW11	260	259.6	0.998	9.8	10.9	1.107
SW12	340	328.4	0.966	9.8	10.0	1.019
SW13	330	352.0	1.067	8.9	11.4	1.284
SW14	265	259.6	0.980	11.2	10.9	0.969
SW15	320	321.5	1.005	8.8	10.0	1.129
SW16	355	354.9	1.000	5.8	6.9	1.197
SW17	247	241.8	0.979	10.8	10.5	0.972
SW21	127	121.7	0.958	20.6	20.0	0.970
SW22	150	148.9	0.993	15.3	14.6	0.954
SW23	180	170.2	0.946	13.2	14.6	1.107
SW24	120	121.7	1.014	18.1	20.0	1.103
SW25	150	164.3	1.095	9.5	13.1	1.383
SW26	123	120.1	0.976	20.9	21.7	1.036
Mean	/	/	0.998	/	/	1.095
C.O.V.	/	/	0.042	/	/	0.131

1.0, and type 2, where such ratio is 2.0. The steel configurations, the vertical loadings and other details of the experimental tests are referred in Lefas et al. (1990) and Vecchio (1992). The material properties of concrete adopted in the simulation were: $E_0 = 30.7$ GPa, $f_0^+ = 3.0$ MPa, $f_0^- = 10.0$ MPa. For both types of shearwalls, 8-node plane stress elements and 2-node truss element are used for modeling the concrete and the steel reinforcement, respectively.

The numerically predicted load–displacement responses agree well with the experimental results, one of which is shown in Fig. 9, reproducing the horizontal force and displacement at the top of the shearwalls SW11 and SW14. The distributions of the tensile damage of SW11 under the horizontal loadings of 122.0 kN and 153.1 kN are shown in Fig. 10, providing useful information about the flexural-shear induced cracking.

For the 13 shearwalls the peak loads and the corresponding displacements computed with the proposed model are compared with the experimental ones in Table 1. It can be clearly seen that the peak forces F and the corresponding displacements U of all the shearwalls are reproduced rather well by the proposed model: (i) the ratio of the numerically predicted peak loads to the experimental ones has a mean value of 0.998 and a coefficient of variation of 0.042, and (ii) the corresponding values for the displacement ratios are 1.095 and 0.131, respectively.

6. Conclusions

This paper presents a damage energy release rate-based plastic-damage constitutive model, mainly intended for the nonlinear analysis of plain and reinforced concrete structures. Within the framework of continuum damage mechanics, two damage scalars that lead to a fourth-order damage tensor are adopted to describe the degradation of the macromechanical properties of concrete. An elegant constitutive law is formulated on the basis of a decomposition of effective stress tensor. The plastic Helmholtz free energy is taken into accounted for the damage growth, and the damage criteria are based on the elastoplastic damage energy release rates.

The numerical predictions from the proposed model when applied to plain concrete and reinforced concrete specimens and structures were checked in several experimental examples, demonstrating the following capabilities:

(1) It is able to reproduce most of the typical nonlinear performances of concrete under monotonic and cyclic load conditions, as well as under 2D or 3D stress states;
(2) It is capable of providing not only the experimentally observed load–deflection response curves, but also the real distributions of structural damages.

Acknowledgement

The project under which this paper was prepared was supported by the National Natural Science Foundation for Outstanding Youth in China (No. 59825105) and the Natural Science Foundations of China for Innovative Research Groups (No. 50321803), which are gratefully acknowledged.

Appendix I. Derivation of the projection tensors of $\bar{\boldsymbol{\sigma}}$ and $\dot{\bar{\boldsymbol{\sigma}}}$

The spectral decomposition of the effective stress tensor proposed in Ortiz (1985) is considered here

$$\bar{\boldsymbol{\sigma}} = \sum_i \bar{\sigma}_i \mathbf{n}_i \otimes \mathbf{n}_i \tag{A-I.1}$$

where $\bar{\sigma}_i$ and $\mathbf{n}_i$ $(i = 1, 2, 3)$ are the extracted effective eigenstresses and the corresponding normalized eigenvectors, which the following properties hold:

$$\mathbf{n}_i \cdot \bar{\boldsymbol{\sigma}} \cdot \mathbf{n}_i = \bar{\sigma}_i; \quad \mathbf{n}_i \cdot \mathbf{n}_j = \delta_{ij} \tag{A-I.2a, b}$$

The positive component of the effective stress tensor $\bar{\boldsymbol{\sigma}}^+$ can be expressed as

$$\bar{\boldsymbol{\sigma}}^+ = \sum_i \langle \bar{\sigma}_i \rangle \mathbf{n}_i \otimes \mathbf{n}_i = \sum_i H(\bar{\sigma}_i) \mathbf{n}_i \otimes \boldsymbol{n}_i \bar{\sigma}_i \tag{A-I.3}$$

Substituting Eq. (A-I.2a) into Eq. (A-I.3), one obtains

$$\bar{\boldsymbol{\sigma}}^+ = \sum_i H(\bar{\sigma}_i) \mathbf{n}_i \otimes \mathbf{n}_i [(\mathbf{n}_i \otimes \mathbf{n}_i) : \bar{\boldsymbol{\sigma}}] = \mathbf{P}^+ : \bar{\boldsymbol{\sigma}} \tag{A-I.4}$$

with the positive projection tensor $\mathbf{P}^+$ being (Faria et al., 2000)

$$\mathbf{P}^+ = \sum_i H(\bar{\sigma}_i)(\mathbf{n}_i \otimes \mathbf{n}_i) \otimes (\mathbf{n}_i \otimes \mathbf{n}_i) \tag{A-I.5}$$

which were already defined in Eqs. (3a) and (4a), accordingly, $\bar{\boldsymbol{\sigma}}^-$ and $\mathbf{P}^-$ defined in Eqs. (3b) and (4b) can thus be easily obtained.

The total differential of Eq. (A-I.3) gives

$$\mathrm{d}\bar{\boldsymbol{\sigma}}^+ = \sum_i H(\bar{\sigma}_i)(\mathbf{n}_i \otimes \mathbf{n}_i)\mathrm{d}\bar{\sigma}_i + \sum_i \langle \bar{\sigma}_i \rangle \mathrm{d}(\mathbf{n}_i \otimes \mathbf{n}_i) \tag{A-I.6}$$

Differentiating of Eq. (A-I.2a), one obtains

$$\mathrm{d}\bar{\sigma}_i = \mathbf{n}_i \cdot \mathrm{d}\bar{\boldsymbol{\sigma}} \cdot \mathbf{n}_i + 2\mathrm{d}\mathbf{n}_i \cdot \bar{\boldsymbol{\sigma}} \cdot \mathbf{n}_i = (\mathbf{n}_i \otimes \mathbf{n}_i) : \mathrm{d}\bar{\boldsymbol{\sigma}} \tag{A-I.7}$$

where Eq. (A-I.2b) is taken into consideration to conclude that the above second right term is equal to zero.

In Faria et al. (2000) the expression for $\mathrm{d}(\mathbf{n}_i \otimes \mathbf{n}_i)$ was derived as

$$\mathrm{d}(\mathbf{n}_i \otimes \mathbf{n}_i) = \mathrm{d}\mathbf{n}_i \otimes \boldsymbol{n}_i + \mathbf{n}_i \otimes \mathrm{d}\mathbf{n}_i = \left[2\sum_{j\neq i} \frac{1}{\bar{\sigma}_i - \bar{\sigma}_j}(\mathbf{p}_{ij} \otimes \mathbf{p}_{ij})\right] : \mathrm{d}\bar{\boldsymbol{\sigma}} \tag{A-I.8}$$

where $\mathbf{p}_{ij}$ is the second-order symmetry tensor defined in Eq. (7).

Substituting Eqs. (A-I.7) and (A-I.8) into Eq. (A-I.6), and after some simple simplifications, $\mathbf{Q}^+$ and $\mathbf{Q}^-$ which are the fourth-order symmetry projection tensor of $\dot{\bar{\boldsymbol{\sigma}}}$, can thus be derived as those expressions defined in Eqs. (6a) and (6b).

Appendix II. Derivation of the plastic and elastoplastic HFE potential

Since the contribution to the HFE potential of plastic strains in tension is neglected in the proposed mode, i.e, $\psi_0^{\mathrm{p}+} = 0$ is assumed, the plastic HFE potential is defined

$$\psi_0^{\mathrm{p}}(\boldsymbol{\kappa}) = \psi_0^{\mathrm{p}-}(\boldsymbol{\kappa}) = \int_0^{\boldsymbol{\varepsilon}^{\mathrm{p}}} \bar{\boldsymbol{\sigma}}^- : \mathrm{d}\boldsymbol{\varepsilon}^{\mathrm{p}} \tag{A-II.1}$$

Substituting Eq. (25) into (A-II.1), and after some simplifications (Wu, 2004), the above initial plastic HFE potential becomes Eq. (36) as

$$\psi_0^{\mathrm{p}} = \frac{b}{2E_0}\left(3\overline{J}_2^- + \eta^{\mathrm{p}}\overline{I}_1^-\sqrt{3\overline{J}_2} - \frac{1}{2}\overline{I}_1^+\overline{I}_1^-\right) \tag{A-II.2}$$

where parameter $b \geqslant 0$ will be determined in the following procedure. If $b = 0$ is assumed, the contribution of plastic HFE would not be taken into consideration.

Calling for Eq. (2) and with v_0 denoting the initial Poisson's ratio, the negative component of the elastic HFE potential defined in Eq. (10b) is rewritten as

$$\psi_0^{\mathrm{e}-} = \frac{1}{2E_0}\left[\frac{2(1+v_0)}{3}3\overline{J}_2^- + \frac{1-2v_0}{3}(\overline{I}_1^-)^2 - v_0\overline{I}_1^+\overline{I}_1^-\right] \tag{A-II.3}$$

Then ψ_0^- defined in Eq. (39b) becomes

$$\psi_0^- = \psi_0^{\mathrm{e}-} + \psi_0^{\mathrm{p}-} = b_0\left[3\overline{J}_2^- + b_1\overline{I}_1^-\sqrt{3\overline{J}_2} + b_2(\overline{I}_1^-)^2 + b_3\overline{I}_1^+\overline{I}_1^-\right] \tag{A-II.4}$$

with parameters b_0, b_1, b_2 and b_3 being

$$b_0 = a/(6E_0); \quad b_1 = 3b\eta^{\mathrm{p}}/a; \quad b_2 = (1-2v_0)/a; \quad b_3 = -1.5(b-2v_0)/a \tag{A-II.5}$$

and $a = 3b + 2(1+v_0)$.

Calling for Eqs. (41) and (A-II.4), under pure compression Y^- can then be reduced to the following expression:

$$Y^- = \psi_0^- = b_0\left[3\overline{J}_2^- + b_1\overline{I}_1^-\sqrt{3\overline{J}_2^-} + b_2(\overline{I}_1^-)^2\right] \tag{A-II.6}$$

Denoting by f_{b0}^- the stresses (positive values) beyond which nonlinearity becomes visible under equibiaxial compression, the initial shear damage threshold r_0^- is thus established as (Wu, 2004)

$$r_0^- = \frac{1}{2E_0}[1 + b(1-\eta^{\mathrm{p}})](f_0^-)^2 = \frac{1}{2E_0}[2(1-v_0) + b(1-2\eta^{\mathrm{p}})](f_{b0}^-)^2 \tag{A-II.7}$$

leading to the following expression for parameter b introduced in Eq. (A-II.2) as

$$b = \frac{1 - 2(1 - \nu_0)\vartheta_0^2}{(1 - 2\eta^{\mathrm{p}})\vartheta_0^2 - (1 - \eta^{\mathrm{p}})} \tag{A-II.8}$$

with $\vartheta_0 = f_{b0}^-/f_0^-$, assumed to take the same value as ϑ defined in Eq. (31a), i.e, $\vartheta_0 = \vartheta$ (Lubliner et al., 1989). For concrete, the following inequality is inherently satisfied:

$$1 - 2(1 - \nu_0)\vartheta^2 < 0 \tag{A-II.9}$$

Owing to the non-negative nature of parameter b, Eqs. (A-II.8) and (A-II.9) lead to the condition that dilatancy parameter α^{p} should fulfill

$$\alpha^{\mathrm{p}} = \sqrt{2/3}\eta^{\mathrm{p}} \geqslant \sqrt{2/3}(\vartheta^2 - 1)/(2\vartheta^2 - 1) \tag{A-II.10}$$

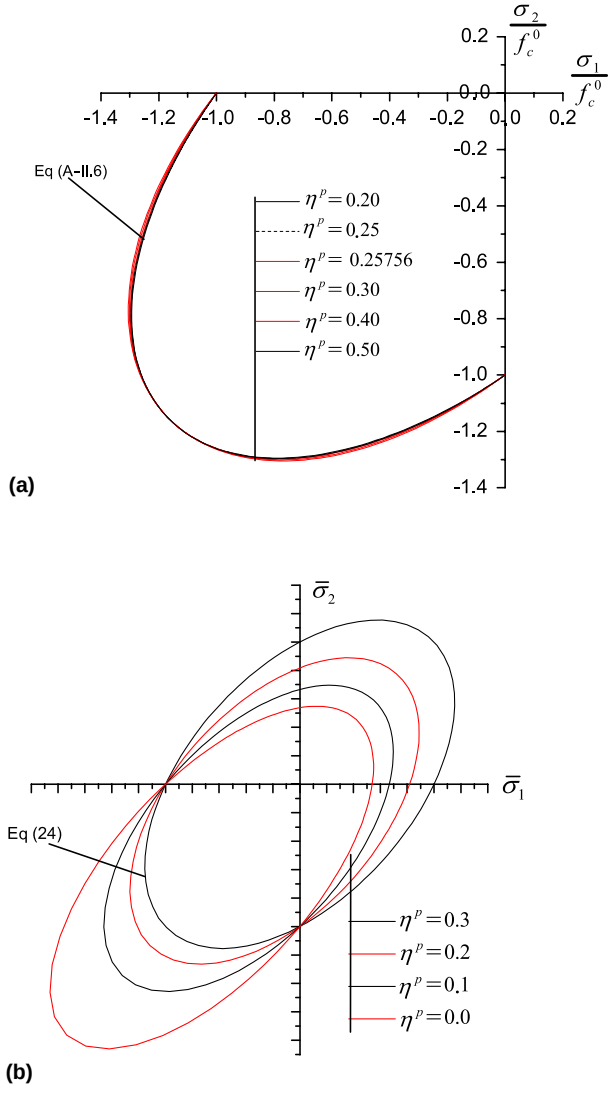

Fig. 11. Influence of parameter η^{p}: (a) domain of linear behaviour under biaxial compression; (b) plastic potential.

Since ratio ϑ usually lies in the interval 1.10–1.20, from Eq. (A-II.10) one gets $\alpha^{\mathrm{p}} \geqslant 0.12$–$0.19$, which can be strictly satisfied since the value of 0.20–0.30 is usually adopted for concrete (Lee and Fenves, 1998).

Taking into consideration Eqs. (A-II.6) and (A-II.7), for different dilatancy parameters η^{p}, the corresponding domains of linear behaviour of concrete under biaxial compression, using the typical parameters $v_0 = 0.2$ and $\vartheta = 1.16$, are shown in Fig. 11; the plastic potential function introduced in Eq. (24), corresponding to different values of η^{p} are also reproduced.

As the dilatancy parameter η^{p} (or α^{p}) has substantial influence on the plastic potential, but almost no effect on the domains of linear behaviour under biaxial compression, it allows great simplifications to be introduced on the shear DERR expressed in Eq. (A-II.6). Let η^{p} take the value of 0.25756, i.e., $\alpha^{\mathrm{p}} = 0.21$, then $b_2 = (b_1/2)^2$ is obtained, and consequently Eq. (A-II.6) can be approximated by the following form of a perfect square polynomial:

$$Y^- = \psi_0^- = b_0\left(\alpha\bar{I}_1^- + \sqrt{3\bar{J}_2^-}\right)^2 \tag{A-II.11}$$

In a tension-included stress states (e.g. tensile-compressive quadrants), according to Eq. (A-II.4) the tensile stresses do have some influence on the domain of linear behaviour, localized in the circle areas close to the tension–compression corners depicted in Fig. 1, whose effect is so subtle that can be ignored. Consequently, the negative component of initial elastoplastic HFE potential ψ_0^- and the corresponding shear DERR Y^- defined in Eq. (A-II.11), can be further approximated as the expression defined in (40b).

It should be noted that the above approximations lead to great simplicity without significant loss of accuracy, and at the same time they ensure the convexity of the damage surfaces, which not only can greatly facilitate its numerical implementation, but also may enhance the numerical stability of the proposed model.

References

Bhattacharjee, S., Leeger, P., 1993. Seismic cracking and energy dissipation in concrete gravity dams. Earthquake Engineering and Structure Dynamics 22, 991–1007.

Carol, I., Rizzi, E., Willam, K., 1994. A unified theory of elastic degradation and damage based on a loading surface. International Journal of Solids and Structures 31 (20), 2853–2865.

Cervera, M., Oliver, J., Faria, R., 1995. Seismic evaluation of concrete dams via continuum damage models. Earthquake Engineering and Structural Dynamics 24, 1225–1245.

Cervera, M., Oliver, J., Manzoli, O., 1996. A rate-dependent isotropic damage model for the seismic analysis of concrete dams. Earthquake Engineering and Structural Dynamics 25, 987–1010.

Chaboche, J.L. et al., 1995. Continuum damage mechanics, anisotropic and damage deactivation for brittle materials like concrete and ceramic composites. International Journal of Damage Mechanics 4.

Chen, W.F., 1994. Constitutive Equations for Engineering Materials—Plasticity and Modeling, vol. 2. Elsevier, Amsterdam.

Chopra, A.K., Chakrabarti, P., 1973. The Koyna earthquake and the damage to Koyna dam. Bulletin of the Seismological Society of America 63 (2), 381–397.

Chow, C.L., Wang, J., 1987. An anisotropic theory of continuum damage mechanics for ductile fracture. Engineering Fracture Mechanics 27, 547–558.

Coleman, B.D., Gurtin, M.E., 1967. Thermodynamics with internal state variables. Journal of Chemistry and Physics 47, 597–613.

Comi, C., Perego, U., 2001. Fracture energy based bi-dissipative damage model for concrete. International Journal of Solids and Structures 38, 6427–6454.

di Prisco, M., Mazars, J., 1996. Crush-crack: a non-local model for concrete. Mechanics of Cohesive-Frictional Materials 1, 321–347.

Dragon, A., 1985. Plasticity and ductile fracture damage: study of void growth in metals. Engineering Fracture Mechanics 21, 875–885.

Etse, G., Willam, K., 1994. Fracture energy formulation for inelastic behaviour of plain concrete. Journal of Engineering Mechanics, ASCE 120, 1983–2011.

Faria, R., Oliver, J., Cervera, M., 1998. A strain-based plastic viscous-damage model for massive concrete structures. International Journal of Solids Structures 35 (14), 1533–1558.

Faria, R., Oliver, J., Cervera, M., 2000. On isotropic scalar damage models for the numerical analysis of concrete structures. CIMNE Monograph, No.198, Barcelona, Spain.

Feenstra, P.H., de Borst, R., 1996. A composite plasticity model for concrete. International Journal of Solids and Structures 33 (6), 707–730.

Geopalaeratnam, V.S., Shah, S.P., 1985. Softening response of plain concrete in direct tension. ACI Journal 85 (3), 310–323.

Ghrib, F., Tinawi, R., 1995. An application of damage mechanics for seismic analysis of concrete gravity dams. Earthquake Engineering and Structural Dynamics 24, 157–173.

Green, S.J., Swanson, S.R., 1973. Static constitutive relations for concrete. AFWL-TR-72-244, US Air Force Weapons Laboratory, Kirtland Air Force Base, NM.

Halm, D., Dragon, A., 1996. A model of anisotropic damage mesocrack growth: unilateral effect. International Journal of Damage Mechanics 5, 384–402.

Hansen, E., Willam, K., Carol, I., 2001. A two-surface anisotropic damage/plasticity model for plain concrete. In: Proceeding of Framcos-4 Conference, Paris.

Hatzigeorgioiu, G. et al., 2001. A simple concrete damage model for dynamic Fem applications. International Journal of Computational Engineering Science 2 (2), 267–286.

Ju, J.W., 1989. On energy-based coupled elastoplastic damage theories: constitutive modeling and computational aspects. International Journal of Solids and Structures 25 (7), 803–833.

Ju, J.W., 1990. Isotropic and anisotropic damage variables in continuum damage mechanics. Journal of Engineering Mechanics, ASCE 116 (12), 2764–2770.

Karson, I.D., Jirsa, J.O., 1969. Behaviour of concrete under compressive loadings. Journal of Structure Division, ASCE 95 (12), 2535–2563.

Krajcinovic, D., 1985. Constitutive theories for solids and structures with defective microstructure. Damage Mechanics and Continuum Modeling, ASCE, 39–56.

Kupfer, H., Hilsdorf, H.K., Rusch, H., 1969. Behaviour of concrete under biaxial stress. Proc. ACI 66, 656–666.

Lee, J., Fenves, G.L., 1998. Plastic-damage model for cyclic loading of concrete structures. Journal of Engineering Mechanics Division, ASCE 124, 892–900.

Lee, J., Fenves, G.L., 2002. A return-mapping algorithm for plastic-damage models: 3-D and plane stress formulation. International Journal of Numerical Methods in Engineering 50, 487–506.

Lefas, D., Kotsovos, M.D., Ambraseys, N.N., 1990. Behaviour of reinforced concrete structural walls: strength, deformation characteristics, and failure mechanism. ACI Structural Journal 87 (1), 23–31.

Lemaitre, J., 1985. A continuum damage mechanics model for ductile fracture. Journal of Engineering Materials Technology 107, 83–89.

Li, J., Wu, J.Y., 2004. Energy-based CDM model for nonlinear analysis of confined concrete structures. In: International Symposium on Confined Concrete (ISCC), June 12–14, Changsha, China.

Lubarda, V.A., Kracjinvovic, D., Mastilovic, S., 1994. Damage model for brittle elastic solids with unequal tensile and compressive strength. Engineering Fracture Mechanics 49 (5), 681–697.

Lubliner, J., 1972. On the thermodynamic foundations of nonlinear solid mechanics. International Journal of Solids and Structures 25 (3), 237–254.

Lubliner, J., Oliver, S., Oñate, E., 1989. A plastic-damage model for concrete. International Journal of Solids and Structures 25 (2), 299–326.

Mazars, J., 1984. Application de la mécanique de l'endommagement au comportement non linéaire et a la rupture du béton de structure. Thèse de Doctorat d' Etat, L.M.T., Université Paris, France.

Mazars, J., 1985. A model of unilateral elastic damageable material and its application to concrete. In: Proceedings of the RILEM International Conference on Fracture Mechanics of Concrete, Lausanne, Switzerland, Elsevier, New York, N. Y. J.

Mazars, J., Pijaudier-Cabot, 1989. Continuum damage theory: application to concrete. Journal of Engineering Mechanics, ASCE 115 (2), 345–365.

McNeice, A.M., 1967. Elastic–plastic bending of plates and slabs by the finite element method. Ph.D. Thesis, London University.

Ohtani, Y., Chen, W.F., 1988. Multiple hardening plasticity for concrete materials. Journal of Engineering Mechanics, ASCE 114, 1890–1910.

Oliver, J., Cervera, M., Oller, S., Lubliner, J., 1990. Isotropic damage models and smeared crack analysis of concrete. In: Proc. 2nd Int. Conf. Comput. Aided Analysis Design Conc. Structures, Zell am See, pp. 945–957.

Ortiz, M., 1985. A constitutive theory for inelastic behaviour of concrete. Mechanics of Materials 4, 67–93.

Resende, L., 1987. A damage mechanics constitutive theory for the inelastic behaviour of concrete. Computer Methods in Applied Mechanics and Engineering 60, 57–93.

Simo, J.C., Hughes, T.J.R., 1998. Computational Inelasticity. Springer-Verlag, New York.

Simo, J.C., Ju, J.W., 1987. Strain- and stress-based continuum damage models-I: formulation. International Journal of Solids and Structures 23 (7), 821–840.

Stevens, N.J. et al., 1991. Constitutive model for reinforced concrete finite element analysis. ACI Structural Journal 88 (1), 49–59.
Taylor, R.L., 1992. FEAP: a finite element analysis program for engineering workstation. Rep. No. UCB/SEMM-92 (Draft Version), Department of Civil Engineering, University of California, Berkeley.
Vecchio, F.J., 1992. Finite element modeling of concrete expansion and confinement. Journal of Engineering Mechanics, ASCE 118 (9), 2390–2406.
Vecchio, F.J., Collins, M.P., 1986. The modified compression-field theory for reinforced concrete elements subjected to shear. ACI Structure Journal 83 (2), 219–231.
Westergaard, H.M., 1933. Water pressures on dams during earthquakes. Transactions of the American Society of Civil Engineers 98, 418–433.
Wu, J.Y., 2004. Damage energy release rate-based elastoplastic damage constitutive model for concrete and its application to nonlinear analysis of structures. Ph.D. Dissertation, Tongji University, Shanghai, China.
Wu, J.Y., Li, J., 2004. A new energy-based elastoplastic damage model for concrete. In: Proceedings of the XXI International Conference of Theoretical and Applied Mechanics (ICTAM), Warsaw, Poland.
Yazdani, S., Schreyer, H.L., 1990. Combined plasticity and damage mechanics model for plain concrete. Journal of Engineering Mechanics, ASCE 116 (7), 1435–1450.
Zhang, Q.Y., 2001. Research on the stochastic damage constitutive of concrete material. Ph.D. Dissertation, Tongji University, Shanghai, China.